Resurrecting essential amino acid biosynthesis in mammalian cells

Julie Trolle[1†], Ross M. McBee[2,3†], Andrew Kaufman[3], Sudarshan Pinglay[1], Henri Berger[1‡], Sergei German[1], Liyuan Liu[3], Michael J. Shen[1,4], Xinyi Guo[5], J. Andrew Martin[1§], Michael Pacold[6], Drew R. Jones[7], Jef D. Boeke[1,8*], Harris H. Wang[3*]

Affiliations:

[1] Institute for Systems Genetics, Department of Biochemistry and Molecular Pharmacology, NYU Langone Health; New York, NY, USA.

[2] Department of Biological Sciences, Columbia University; New York, NY, USA.

[3] Department of Systems Biology, Columbia University; New York, NY, USA.

[4] Department of Internal Medicine, NYU Langone Health; New York, NY, USA.

[5] Department of Biology, New York University; New York, NY, USA.

[6] Department of Radiation Oncology, NYU Langone Health; New York, NY, USA.

[7] Department of Biochemistry and Molecular Pharmacology, NYU Langone Health; New York, NY, USA.

[8] Department of Biomedical Engineering, NYU Tandon School of Engineering; Brooklyn, NY 11201, USA.

† These authors contributed equally to this work

* Correspondence should be addressed to hw2429@columbia.edu or jef.boeke@nyulangone.org

‡ Current address: Weill Cornell Graduate School of Medical Sciences; New York, NY, USA.

§ Current address: Reopen Diagnostics, LLC; Queens, NY, USA.

ABSTRACT

Major genomic deletions in independent eukaryotic lineages have led to repeated ancestral loss of biosynthesis pathways for nine of the twenty canonical amino acids[1]. While the evolutionary forces driving these polyphyletic deletion events are not well understood, the consequence is that extant metazoans are unable to produce nine essential amino acids (EAAs). Previous studies have highlighted that EAA biosynthesis tends to be more energetically costly[2,3], raising the possibility that these pathways were lost from organisms with access to abundant EAAs in the environment[4,5]. It is unclear whether present-day metazoans can reaccept these pathways to resurrect biosynthetic capabilities that were lost long ago or whether evolution has rendered EAA pathways incompatible with metazoan metabolism. Here, we report progress on a large-scale synthetic genomics effort to reestablish EAA biosynthetic functionality in mammalian cells. We designed codon-optimized biosynthesis pathways based on genes mined from *Escherichia coli*. These pathways were *de novo* synthesized in 3 kilobase chunks, assembled *in yeasto* and genomically integrated into a Chinese Hamster Ovary (CHO) cell line. One synthetic pathway produced valine at a sufficient level for cell viability and proliferation, and thus represents a successful example of metazoan EAA biosynthesis restoration. This prototrophic CHO line grows in valine-free medium, and metabolomics using labeled precursors verified *de novo* biosynthesis of valine. RNA-seq profiling of the valine prototrophic CHO line showed that the synthetic pathway minimally disrupted the cellular transcriptome. Furthermore, valine prototrophic cells exhibited transcriptional signatures associated with rescue from nutritional starvation. ^{13}C-tracing revealed build-up of pathway intermediate 2,3-dihydroxy-3-isovalerate in these cells. Increasing the dosage of downstream *ilvD* boosted pathway performance and allowed for long-term propagation of second-generation cells in valine-free medium at a consistent doubling time of 3.2 days. This work demonstrates that mammalian metabolism is amenable to restoration of ancient core pathways, paving a path for genome-scale efforts to synthetically restore metabolic functions to the metazoan lineage.

MAIN TEXT

Whole genome sequencing across the tree of life has revealed the surprising observation that nine amino acid (AA) biosynthesis pathways are missing from the metazoan lineage[1]. Furthermore, these losses appear to have occurred multiple times during eukaryotic evolution, including in some microbial lineages (**Fig 1A**)[1,4]. Branching from core metabolism, the nine EAA

biosynthesis pathways missing from metazoans involve over forty genes (**Fig 1B, Supplementary files 1-3**) that are widely found in bacteria, fungi and plants[4]. While the absence of pathways that produce essential metabolites is observed in certain bacteria[6], which possess short generation times and high genomic flexibility to adapt to rapidly changing environments, the forces driving the loss of multiple EAA biosynthetic pathways in multicellular eukaryotes remain a great mystery. An exception that proves the rule is the partial reacquisition of EAA biosynthetic pathways through horizontal gene transfer in certain rare insect lineages which host genome-reduced intracellular bacteria and feed on simple nutrient sources such as sap or blood[7]. Recent efforts in genome-scale synthesis[8–10] and genome-writing[11] have highlighted our increasing capacity to construct synthetic genomes with novel properties, thus providing a route to not only examine these interesting evolutionary questions but also yield new capacities of bioindustrial utility[12–14].

We sought to explore the possibility of generating prototrophic mammalian cells capable of complete biosynthesis of EAAs using a synthetic genomics approach (**Fig 1C**). The Chinese Hamster Ovary (CHO) K1 cell line was chosen as a model system due to its fast generation time, amenability to genetic manipulations, availability of a whole genome sequence, and established industrial relevance for producing biologics[15]. EAA biosynthesis genes from the best characterized model organisms were considered during pathway design while optimizing for the fewest number of enzymes needed for a given EAA pathway. To avoid using multiple promoters, we introduced ribosome-skipping 2A sequences[16] between biosynthetic genes to allow for protein translation of separate enzymes from a single transcriptional unit. The EAA pathway and an additional EGFP reporter were placed in a vector that could be integrated as a single copy into the CHO genome at a designated landing pad using the Flp-In system[17]. The entire pathway was synthesized *de novo* by commercial gene synthesis in 3 kilobase fragments and assembled in *Saccharomyces cerevisiae* via homologous recombination of 80-basepair overlaps. Subsequent antibiotic selection of cells transfected with the vector resulted in a stable cell line containing the integrated EAA pathway. Finally, we performed a variety of phenotypic, metabolomic, and transcriptomic characterizations on the modified cell line to verify activity of the EAA biosynthesis pathway.

We first confirmed that the CHO cell line was in fact auxotrophic for each of the 9 EAAs. As expected, CHO-K1 did not grow in “dropout” F-12K medium lacking each of the 9 EAAs and supplemented with dialyzed FBS (**Figure 1 – figure supplement 1).** We noted that in this cell line, canonically non-essential amino acids tyrosine and proline also exhibited EAA-like properties in dropout media. Insufficient concentrations of phenylalanine in F-12K medium or

low expression of endogenous phenylalanine-4-hydroxylase that converts phenylalanine to tyrosine could underlie the tyrosine limitation. Proline auxotrophy in CHO-K1 results from epigenetic silencing of the gene encoding Δ1-pyrroline-5-carboxylate synthetase (P5CS) in the proline pathway[18]. We therefore used proline as a test case for our synthetic genomics pipeline. We tested the P5CS-equivalent proline biosynthesis enzyme found in *E. coli*, encoded by two separate genes, *proA* and *proB* (**Figure 1 – figure supplement 2A**). A vector (pPro) carrying codon-optimized *proA* and *proB* separated by a P2A sequence was synthesized and integrated into CHO-K1 (**Figure 1 – figure supplement 2B**). CHO cells with the stably integrated pPro proline pathway showed robust growth in proline-free F-12K medium (**Figure 1 – figure supplement 2C-D**), thus validating a pipeline for designing and generating specific AA prototrophic cells.

To demonstrate restoration of EAA pathways lost from the metazoan lineage more than 650-850 million years ago[19], we built a 6-gene construct (pMTIV) to investigate the potential rescue of methionine, threonine, isoleucine and valine auxotrophies. These EAAs were chosen because their biosynthesis pathways were missing the fewest number of genes. Valine and isoleucine collectively require four genes to recapitulate the bacterial-native pathway. (**Figure 2 – figure supplement 1**). The two remaining genes were included to test potential routes to simultaneously rescue threonine and methionine auxotrophy by selectively supplementing individual missing metabolic steps, in addition to complete pathway reconstruction for valine and isoleucine. To biosynthesize methionine, we chose the *E. coli metC* gene, which encodes cystathionine-ß-lyase and converts cystathionine to homocysteine, a missing step in CHO-K1 cells in a potential serine to methionine biosynthetic pathway. Threonine production was tested using *E. coli* L-threonine aldolase *ltaE*, which converts glycine and acetaldehyde into threonine. For branched chain amino acids (BCAAs) valine and isoleucine, three additional biosynthetic enzymes and one regulatory subunit are needed in theory to convert pyruvate and 2-oxobutanoate into valine and isoleucine, respectively. In the case of valine, pyruvate is converted to 2-acetolactate, then to 2,3-dihydroxy-isovalerate, then to 2-oxoisovalerate and finally to valine. For isoleucine, 2-oxobutanoate is converted to 2-aceto-2-hydroxybutanoate, then to 2,3-dihydroxy-3-methylpentanoate, then to 3-methyl-2-oxopentanoate, and finally to isoleucine. The final steps in the biosynthesis of both BCAAs can be performed by native CHO catabolic enzymes Bcat1 and Bcat2[18]. In *E. coli*, the first three steps in the pathway are embodied in four genes that encode an acetolactate synthase with catalytic and regulatory subunits (*ilvB/N*), a ketol-acid reductoisomerase (*ilvC*), and a dihydroxy-acid dehydratase (*ilvD*) (**Fig 2A**)[20]. The final pMTIV construct comprises *metC*, *itaE*, *ilvN, ilvB*, *ilvC* and *ilvD*, organized

as a single open reading frame (ORF) with a 2A sequence variant lying between each protein coding region (**Fig 2B**), and driven by a single strong SFFV viral promoter.

To test the biosynthetic capacity of pMTIV, we first introduced the construct into CHO cells. Flp-In integration was used to stably insert either pMTIV, or a control vector (pCtrl) into the CHO genome. Successful generation of each cell line was confirmed by PCR amplification of junction regions formed during vector integration (**Figure 2 – figure supplement 2A-B**). RNA-seq of cells containing the pMTIV construct confirmed transcription of the entire ORF (**Fig 2B**). Western blotting of pMTIV cells using antibodies against the P2A peptide yielded bands at the expected masses of P2A-tagged proteins, confirming the production of separate distinct enzymes (**Figure 2 – figure supplement 2C**).

In reconstituted methionine-free, threonine-free, or isoleucine-free F-12K medium supplemented with dialyzed FBS to reduce FBS-derived AA content (**Figure 2 – figure supplement 3),** cells containing the pMTIV construct did not show viability over seven days, similar to cells containing the pCtrl control vector (**Figure 2 – figure supplement 4**). In striking contrast, however, cells containing the integrated pMTIV showed relatively healthy cell morphology and viability in valine-free F-12K medium (**Fig 2C**), whereas cells containing pCtrl exhibited substantial loss of viability over six days. In complete F-12K medium, cells carrying the integrated pMTIV construct showed no growth defects compared to control cells (**Fig 2D**). In valine-free F-12K medium, pMTIV cells showed a 32% increase in cell number over 6 days compared to an 88% decrease in cell number in pCtrl cells (**Fig 2E**). When cultured in valine-free F-12K medium over multiple passages with medium changes every two days, pMTIV cell proliferation was substantially reduced by the 3rd passage. We hypothesized that frequent passaging might over-dilute the medium and prevent sufficient accumulation of biosynthesized valine necessary for continued proliferation as has been demonstrated for certain non-essential metabolites which become essential when cells are cultured at low cell densities[21]. We thus deployed a “conditioned-medium” regimen whereby 50% of the medium was freshly prepared valine-free F-12K medium and 50% was “conditioned” valine-free F-12K medium in which pMTIV cells had previously been cultured over 2 days (see Methods). While use of pMTIV-conditioned medium improved the survival of cells harboring the pathway, it did not completely rescue valine auxotrophy in control cells, which exhibited substantial loss of cell viability over 8 days (**Figure 2 – figure supplement 5A**). As a control, we generated pCtrl-conditioned valine-free F-12K medium using the same medium conditioning regimen, which failed to enable cells to grow to the same degree as that of pMTIV-conditioned medium, suggesting that the benefit conferred by medium conditioning is valine-specific (**Figure 2 – figure supplement 5B**). Using

this regimen, we were able to culture pMTIV cells for 9 passages without addition of exogenous valine (**Fig 2F**). The doubling time was inconsistent across the 49 days of experimentation with cells exhibiting a mean doubling time of 5.3 days in the first 24 days and 21.0 days in the last 25 days. Despite the slowed growth seen in later passages, cells exhibited healthy morphology and continued viability at day 49, suggesting that the cells could have been passaged even further. To verify that the putative valine rescue effect was due to the valine biosynthesis genes present in pMTIV specifically and did not involve confounding effects due to the threonine and methionine biosynthesis genes included in the pMTIV pathway, we constructed and tested a second EAA pathway vector, "pIV," that only contained the four genes *ilvNBCD*. The pIV construct similarly supported cell growth in valine-free F-12K medium, and exhibited similar growth dynamics to the pMTIV construct in complete medium (**Figure 2 – figure supplement 6**).

To confirm endogenous biosynthesis of valine, we cultured pCtrl and pMTIV cells in RPMI medium containing $^{13}C_6$-glucose in the place of its ^{12}C equivalent together with $^{13}C_3$-sodium pyruvate spiked in at 2 mM over 3 passages (**Figure 3 – figure supplement 1A**). High-resolution MS1 of MTIV cell lysates revealed a peak at 123.1032 *m*/*z*, the expected *m*/*z* for $^{13}C_5$-valine (**Fig 3A**). This detected peak was subject to MS2 alongside a ^{12}C-valine control peak and a $^{13}C_5/^{15}N$-valine peak, which was spiked into all samples to serve as an internal standard. The resulting fragmentation patterns for each peak (**Fig 3B**) matched theoretical expectations for each isotopic version of valine (**Figure 3 – figure supplement 1B**). An extracted ion chromatogram further revealed a peak in the pMTIV valine-free medium metabolite extraction, which corresponded to a peak in the spiked-in positive control $^{13}C_5/^{15}N$-valine, whereas no equivalent peak was seen among metabolites extracted from pCtrl cells (**Figure 3 – figure supplement 1C**). Taken together, this demonstrates that pMTIV cells are capable of biosynthesizing valine from core metabolites glucose and pyruvate, thereby proving successful metazoan biosynthesis of valine. Over the course of 3 passages in heavy valine-free medium, the non-essential amino acid alanine, which is absent from RPMI medium and synthesized from pyruvate, was found to be 86.1% ^{13}C-labeled in pMTIV cell lysates. Assuming similar turnover rates for alanine and valine within the CHO proteome, we expected to see similar percentages of ^{13}C-labeled valine. However, just 32.2% of valine in pMTIV cell lysates was ^{13}C-labeled (**Figure 3 – figure supplement 1D-E**). For pMTIV cells cultured in heavy but valine-replete medium, just 6.4% of valine in cell lysates was ^{13}C-labeled. Together with the observed slow proliferation of pMTIV cells in valine-free medium, our data suggests that valine complementation is sufficient but sub-optimal for cell growth.

We performed RNA-seq to profile the transcriptional responses of cells containing pMTIV or pCtrl in complete (harvested at 0 h) and valine-free F-12K medium (harvested at 4 and 48 h, respectively) (**Fig 3C, Figure 3 – figure supplement 2A**). The transcriptional impact of pathway integration is modest (**Fig 3D**). Only 51 transcripts were differentially expressed between pCtrl and pMTIV cells grown in complete medium, and the fold changes between conditions were small (**Fig 3E, Figure 3 – figure supplement 2B**). While some gene ontology (GO) functional categories were enriched (**Figure 3 – figure supplement 2C**), they did not suggest dramatic cellular stress. Rather, these transcriptional changes may reflect cellular response to BCAA dysregulation due to altered valine levels[22], or may result from cryptic effects of bacterial genes placed in a heterologous mammalian cellular context. In contrast, comparison of 48 h valine-starved pCtrl and pMTIV cells yielded ~7,500 differentially expressed genes. Transcriptomes of pMTIV cells in valine-free medium more closely resembled cells grown on complete medium than did pCtrl cells in valine-free medium (**Fig 3D, Figure 3 – figure supplement 3A)**. Differentially expressed genes between pCtrl and pMTIV cells showed enrichment for hundreds of GO categories, including clear signatures of cellular stress such as autophagy, changes to endoplasmic reticulum trafficking, and ribosome regulation (**Figure 3 – figure supplement 3B**). Most of the differentially regulated genes between pCtrl cells in complete medium, and those same cells starved of valine for 48 hours were also differentially expressed when comparing pCtrl and pMTIV cells in valine-free medium (**Fig 3E**), supporting the hypothesis that most of the observed transcriptional changes represent broad but partial rescue of the cellular response to starvation. We also examined the Integrated Stress Response (ISR) and mTOR signaling pathways, both of which are known to modulate cellular responses to starvation[23]. We observed no clear signatures of mTOR activation (**Figure 3 – figure supplement 4A**), although a number of individual genes related to the mTOR pathway were significantly differentially expressed compared to pCtrl cells valine-starved for 48 h (**Figure 3 – figure supplement 4B)**. A manually curated list of ISR genes showed signals of ISR gene activation, but showed few differences between pCtrl and pMTIV cells at 48 h of starvation (**Figure 3 – figure supplement 4C)**. pMTIV cells grown for 5 passages over 29 days on conditioned valine-free F-12K medium were more similar to pMTIV cells starved for 48 h than to pCtrl cells starved for 48 h (**Figure 3 – figure supplement 5A**). The transcriptomic signature of these cells, appears slightly orthogonal to the “starvation” effect and recovery of pMTIV and pCtrl cells starved for 48 hours in PCA space (**Figure 3 – figure supplement 5B**), but the majority of the differently expressed genes between pMTIV cells starved for 29 days compared to pCtrl cells grown on complete media are shared with cells starved for 48 h (**Figure 3 – figure**

supplement 5C), suggesting some limited cellular adaptation to long term passaging on valine-free media.

To improve rescue of the valine starvation phenotype, we looked for valine biosynthetic pathway intermediates in our metabolomics data that might suggest that the pathway was bottlenecked at any stage. While no signal could be detected for pyruvate, 2-acetolactate or 2-oxoisovalerate, a signal was detected for pathway intermediate $^{13}C_5$-2,3-dihydroxy-isovalerate, which was specific to pMTIV cells cultured in both complete and in valine-free medium (**Fig 3 – figure supplement 1F**). To determine whether the downstream pathway gene, *ilvD*, which encodes the dihydroxy-acid dehydratase enzyme, might constitute a bottleneck, we generated a lentivirus encoding a puromycin resistance cassette in addition to *ilvD* under control of a viral MMLV promoter (**Fig 4A**). Both pCtrl and pMTIV cells were infected and integrants were selected for on puromycin, resulting in a population-averaged integration count of 5.7 copies of *ilvD* for pCtrl cells and 7.1 for pMTIV cells. This resulted in a 0.27 and 0.54 fold increase in *ilvD* expression (measured as a proportion of uninfected pMTIV *ilvD* expression) for infected pCtrl (pCtrl-ilvD+) and infected pMTIV cells (pMTIV-ilvD+), respectively (**Fig 4B**).

We characterized pMTIV and pMTIV-ilvD+ cells by culturing these in isotopically heavy valine-free RPMI medium containing $^{13}C_6$-glucose as before; however, in this experiment 2 mM ^{12}C sodium pyruvate was spiked into the medium rather than ^{13}C-sodium pyruvate (**Figure 4 – figure supplement 1A**). We also reduced the isoleucine content of this isotopically heavy valine-free RPMI medium to match the isoleucine content of F-12K medium from 0.38 mM to 0.06 mM after observing that pMTIV cells proliferated faster in this condition, presumably due to the high sensitivity of the *ilvN/B*-encoded acetolactate synthase complex to isoleucine-induced negative feedback inhibition[24] (**Figure 4 – figure supplement 1B**). pMTIV and pMTIV-ilvD+ cells were cultured in this reduced-isoleucine heavy medium over 36 days on plates coated with 0.1% gelatin (**Figure 4 – figure supplement 1C**). We collected duplicate samples at 6 and 10 different timepoints for pMTIV and pMTIV-ilvD+, respectively, throughout the 36 days of culture. Metabolomics analysis revealed ^{13}C-valine labeling with most of the valine in both pMTIV and pMTIV-ilvD+ cells carrying 0, 2, 3 or 5 ^{13}C carbons at both an early (2 days) and a late (24 days) time point in accordance with the expectation when both $^{12}C_3$ and $^{13}C_3$-pyruvate (derived from $^{13}C_6$-glucose) are present (**Figure 4C**). In pMTIV cells, presence of pathway intermediate 2,3-dihydroxy-isovalerate fluctuated throughout the 24 days of culture with cells exhibiting higher concentrations in earlier time points. In contrast, little or no 2,3-dihydroxy-isovalerate was detected in pMTIV-ilvD+ cells across the entire time course, suggesting that the introduction of the extra copies of *ilvD* is addressing a pathway bottleneck as hypothesized (**Fig 4D**). In pMTIV-

ilvD+ cells, the percentage of valine carrying at least one ^{13}C-labeled carbon also remained relatively steady throughout the 36 days, while pMTIV cells again exhibited more variability (**Fig 4 – figure supplement 1D**). We calculated the molar content of valine within the cells by relativizing peaks to that of the ^{13}C/^{15}N-valine internal standard, which was spiked into each sample at a known concentration. pMTIV samples on average contained 352.0 picomoles of valine per million cells of which 212.5 picomoles was ^{13}C-labeled whereas pMTIV-ilvD+ samples on average contained 423.0 picomoles of valine per million cells of which 242.5 picomoles was ^{13}C-labeled (**Fig 4E**). Collectively, the stabilization of 2,3-dihydroxy-isovalerate and valine levels in pMTIV-ilvD+ cells suggests that the introduction of additional *ilvD*-encoded dihydroxy-acid dehydratases is indeed improving flux through the pathway, allowing cells to respond to low valine levels more efficiently compared to pMTIV cells, which results in a more homeostatic cell state.

We quantified the functional impact of modifying flux at this pathway bottleneck by culturing both cell lines in unconditioned, reduced-isoleucine, valine-free RPMI medium containing 2 mM sodium pyruvate over 10 passages on plates not coated with gelatin. When cultured in this medium, pCtrl-ilvD+ cells displayed rapid loss of cell viability similar to pCtrl cells **(Figure 5 – figure supplement 1A)**. However, pMTIV-ilvD+ cells displayed an improved growth phenotype compared to pMTIV cells with an average doubling time of 3.2 days across 39 days and an apparent ability to proliferate indefinitely (**Fig 5**). By comparison, pMTIV cells exhibited an average doubling time of 4.3 days across 19 days after which they displayed loss of cell viability following passaging events despite both cell lines exhibiting comparable doubling times in complete medium (**Figure 5 – figure supplement 1B**).

In this work, we demonstrated the successful restoration of an EAA biosynthetic pathway in a metazoan cell. Our results indicate that contemporary metazoan biochemistry can support complete biosynthesis of valine, despite millions of years of evolution from its initial loss from the ancestral lineage. Interestingly, independent evidence for BCAA biosynthesis has also been obtained for sap-feeding whitefly bacteriocytes that host bacterial endosymbionts; metabolite sharing between these cells is predicted to lead to biosynthesis of BCAAs that are limiting in their restricted diet. The malleability of mammalian metabolism to accept heterologous core pathways opens up the possibility of animals with designer metabolisms and enhanced capacities to thrive under environmental stress and nutritional starvation[25]. Yet, our failure to functionalize designed methionine, threonine and isoleucine pathways highlights outstanding challenges and future directions for synthetic metabolism engineering in animal cells and animals. Other pathway components or alternative selections may be needed for different

EAAs[26]. For instance, the *ilvB/N* enzyme pair we chose to encode the acetolactate synthase complex in our construct shows feedback sensitivity to isoleucine, which may account for the failure of the pathway to rescue isoleucine auxotrophy. A general lack of predictability and a dearth of well-characterized and controllable genetic "parts" with high dynamic range continue to hamper efforts in genome-scale mammalian engineering[27–29]. Studies to reincorporate EAAs into the core mammalian metabolism could provide greater understanding of nutrient-starvation in different physiological contexts including the tumor microenvironment[30], help answer deep evolutionary questions regarding the formation of the metazoan lineage[31], and lead to new model systems or even therapeutics to address metabolic syndrome, Maple Syrup Urine Disease[32] and Phenylketonuria[33], all of which involve amino acid biosynthetic dysfunction[34,35]. Emerging synthetic genomic efforts to build a prototrophic mammal may require reactivation of many more genes (**Supplementary files 1-3**), iterations of the design, build, test (DBT) cycle, and a larger coordinated research effort to ultimately bring such a project to fruition.

MATERIALS AND METHODS

Key Resources Table

Reagent type (species) or resource	Designation	Source or reference	Identifiers	Additional information
strain, strain background (E. coli)	TransforMax EPI300	Lucigen	C300C105	Chemically competent
strain, strain background (E. coli)	NEB 10-beta	New England Biolabs	C3020K	Electrocompetent
cell line (C. griseus)	CHO Flp-In	ThermoFisher	R75807	
cell line (C. griseus)	CHO pMTIV	This paper		Cell line maintained in J.D.Boeke lab
cell line (C. griseus)	CHO pCtrl	This paper		Cell line maintained in J.D.Boeke lab

cell line (C. griseus)	CHO pMTIV-ilvD+	This paper		Cell line maintained in J.D.Boeke lab
cell line (C. griseus)	CHO pCtrl-ilvD+	This paper		Cell line maintained in J.D.Boeke lab
cell line (C. griseus)	CHO pPro	This paper		Cell line maintained in H.H.Wang lab
cell line (C. griseus)	CHO pCtrl-mCh	This paper		Cell line maintained in H.H.Wang lab
Recombinant DNA reagent	pJTR0381 (plasmid)	This paper		Encodes Ec *ilvD* transcription units for lentiviral transduction
antibody	Anti-2A peptide (mouse monoclonal)	Novus Biologicals	NBP2-59627	1:1000 dilution
antibody	Anti-α/β-tubulin (**r**abbit polyclonal)	Cell Signaling Technology	2148	1:1000 dilution
antibody	IRDye 800CW Anti-mouse IgG (goat polyclonal)	LI-COR	926-32210	1:20000 dilution
antibody	IRDye 680 RD Anti-rabbit IgG (goat polyclonal)	LI-COR	926-68071	1:20000 dilution
commercial assay or kit	PrestoBlue Cell Viability Reagent	ThermoFisher	A13261	
commercial assay or kit	NEBNext poly(A) mRNA Magnetic Isolation module	New England Biolabs	E7490	
commercial assay or kit	NEBNext Ultra RNA Library Prep Kit for	New England Biolabs	E7770	

	Illumina			
other	F-12K medium without amino acids, powder base	US Biological	N8545	Dropout medium base
other	RPMI 1640 without amino acids & glucose, powder base	US Biological	R9010-01	Dropout medium base
other	Gibco fetal bovine serum, dialyzed	Fisher Scientific	26400044	Lot 2140178

313
314

315 Pathway completeness analysis

316 For pathway completeness analysis, the EC numbers of each enzyme in each amino acid
317 biosynthesis pathway (excluding pathways annotated as only occurring in prokaryotes) were
318 collected from the MetaCyc database (**Supplementary file 4**). Variant biosynthetic routes to the
319 same amino acid were considered as separate pathways, generating distinct EC number lists.
320 The resulting per-pathway EC number lists were checked against the KEGG, Entrez Gene,
321 Entrez Nucleotide, and Uniprot databases using their respective web APIs for each listed
322 organism. If the combination of all databases contained at least one complete EC numbers list,
323 corresponding to an end-to-end complete biosynthetic pathway, the organism was considered
324 “complete” for that essential amino acid.

325

326 Cell lines and media

327 CHO Flp-In^{TM} cells (ThermoFisher, R75807) were used in all experiments. All cell lines tested
328 negative for mycoplasma. For growth assays involving amino acid dropout formulations,
329 medium was prepared from an amino acid-free Ham’s F-12 (Kaighn’s) powder base (US
330 Biological, N8545), and custom combinations of amino acids were added back in as needed to
331 match the standard amino acid concentrations for Ham’s F-12 (Kaighn’s) medium or as
332 specified. Custom amino acid dropout medium was adjusted to a pH of 7.3, sterile filtered, and
333 supplemented with 10% dialyzed Fetal Bovine Serum (Fisher Scientific, 26400044) and
334 Penicillin-Streptomycin (100U/mL) prior to use. For metabolomics experiments, medium was

prepared from an amino acid-free and glucose-free RPMI 1640 powder base (US Biological, R9010-01), and custom combinations of amino acids and isotopically heavy glucose and sodium pyruvate were added in to match the standard amino acid concentrations for RPMI 1640 or as specified. pH was adjusted to 7.3, sterile filtered and supplemented with 10% dialyzed Fetal Bovine Serum and Penicillin-Streptomycin (100U/mL) prior to use. Where specified, cells were cultured on plates coated with 0.1% gelatin (EMD Millipore, ES-006-B) for 30 minutes at room temperature. Plates were washed with PBS prior to use.

Cell counting and quantification

For evaluating effects of amino acid dropout on cell growth curves, cells were seeded at $1x10^4$ into 6-well plates into F12-K media with lowered amino acid concentrations relative to typical F12-K media and then allowed to grow for five days. Media was then aspirated off and replaced with PBS with Hoechst 33342 live nuclear stain for automated imaging and counting using a DAPI filter set on an Eclipse Ti2 automated inverted microscope. To count, an automated microscopy routine was used to image 5 random locations within each well at 10x magnification, and then the cells present in imaged frames counted using automatic cell segregation and counting software. Given differences in cell response to starvation, segregation and counting parameters were tuned in each experiment, but kept constant between starvation conditions and cells with and without the pathway. For synthetic prototroph pathway tests, raw cell counts were performed using the Countess II Automated Cell Counter (ThermoFisher, A27977) in accordance with the manufacturer's protocol, or using the Scepter 2.0 Handheld Automated Cell Counter (Millipore Sigma, C85360) in accordance with the manufacturer's protocol. Where indicated, relative cell quantification was measured using PrestoBlue™ Cell Viability Reagent (ThermoFisher, A13261) in accordance with the manufacturer's protocol.

Cell culture in conditioned medium

Conditioned medium was generated by seeding $1x10^6$ pMTIV cells into 10mL complete F12-K medium on 10cm plates and replacing the medium with 10mL freshly prepared valine-free F12-K medium the next day following a PBS wash step. Cells conditioned the medium for 2 days at which point the medium was collected, centrifuged at 300xg for 3 mins to remove potential cell debris, sterile filtered, and collected in 150mL vats to reduce batch-to-batch variation. This 100% conditioned medium was subsequently mixed in a 1:1 ratio with freshly prepared, unconditioned valine-free medium to generate so-called 50% conditioned valine-free medium,

which was used throughout the long-term culturing process of synthetic prototrophic cells without exogenous supply of valine where specified.

DNA assembly, recovery and amplification

Integrated constructs were synthesized *de novo* in 3kb DNA segments with each segment overlapping neighboring segments by 80 bp. Assembly was conducted *in yeasto* by co-transformation of segments into *Saccharomyces cerevisiae* strain BY4741 made competent by the LiOAc method[36]. After 2 days of selection at 30˚C on SC–Ura medium, individual colonies were picked and cultured overnight. 1.5mL of each resulting yeast culture was resuspended in 250µl P1 resuspension buffer (Qiagen, 19051) containing RNase. Glass beads were added to each resuspension and the mixture was vortexed for 10 mins to mechanically shear the cells. Next, cells were subject to alkaline lysis by adding 250µl of P2 lysis buffer (Qiagen, 19052) for 5 mins and then neutralized by addition of Qiagen N3 neutralization buffer (Qiagen, 19053). Subsequently, cell debris was spun down and plasmid DNA was collected using the Zymo Zyppy plasmid preparation kit (Zymo Research, D4036) according to the manufacturer's instructions. Plasmid DNA was eluted in Zyppy Elution buffer and subsequently transformed into TransforMax EPI300 chemically competent *E. coli* in accordance with the manufacturer's protocols (Lucigen, C300C105) for plasmid amplification.

Protein extraction and western blot

Cell were lysed in SKL Triton lysis buffer (50 mM Hepes pH7.5, 150 mM NaCl, 1 mM EDTA, 1 mM EGTA, 10% glycerol, 1% Triton X-100, 25 mM NaF, 10 µM $ZnCl_2$) supplemented with protease inhibitor (Sigma 11873580001). NuPAGE™ LDS sample buffer (ThermoFisher, NP0007) supplemented with 1.43 M β-mercaptoethanol was added to samples prior to heating at 70˚C for 10 mins. Gel electrophoresis was performed using 4-12% Bis-Tris gels (ThermoFisher, NP0326BOX) and run in NuPAGE™ MOPS running buffer (ThermoFisher, NP0001). Proteins were then transferred onto a PVDF membrane (Milipore Sigma, IPFL00010) using the Biorad Trans-Blot Turbo system in accordance with the manufacturer's instructions. The transfer membrane was blocked in Odyssey blocking buffer (LI-COR, 927-40000) for 1 h at room temperature prior to incubation in primary antibody (Novus Biologicals, NBP2-59627 [1:1000 dilution]; Cell Signaling Technology, 2148 [1:1000 dilution]) solubilized in a 1:1 mixture of Odyssey blocking buffer and TBS-T buffer (50 mM Tris Base, 154 mM NaCl, 0.1% Tween20) overnight at 4˚C. Secondary antibodies (LI-COR, 926-32210 [1:20,000 dilution]; LI-COR, 926-

68071 [1:20,000 dilution]),were also solubilized in Odyssey blocking buffer / TBS-T buffer. The membrane was incubated in the secondary antibody solution for 1.5 h at room temperature.

Metabolomics

Cells were cultured in RPMI medium containing ^{13}C-glucose and/or ^{13}C-sodium pyruvate where indicated prior to cell harvest. Cell pellets were generated by trypsinization, followed by low speed centrifugation, and the pellet was frozen at -80˚C until further processing. A metabolite extraction was carried out on each sample with an extraction ratio of 1e6 cells per mL (80% methanol containing internal standards, 500 nM), according to a previously described method[37]. The LC column was a Millipore™ ZIC-pHILIC (2.1 x150 mm, 5 µm) coupled to a Dionex Ultimate 3000™ system and the column oven temperature was set to 25°C for the gradient elution. A flow rate of 100 µL/min was used with the following buffers; A) 10 mM ammonium carbonate in water, pH 9.0, and B) neat acetonitrile. The gradient profile was as follows; 80-20%B (0-30 min), 20-80%B (30-31 min), 80-80%B (31-42 min). Injection volume was set to 1 µL for all analyses (42 min total run time per injection). MS analyses were carried out by coupling the LC system to a Thermo Q Exactive HF™ mass spectrometer operating in heated electrospray ionization mode (HESI). Method duration was 30 min with a polarity switching data-dependent Top 3 method for both positive and negative modes, and targeted MS2 scans for the monoisotopic, U-^{13}C, and U-^{13}C/U-^{15}N valine *m*/*z* values. Spray voltage for both positive and negative modes was 3.5kV and capillary temperature was set to 320°C with a sheath gas rate of 35, aux gas of 10, and max spray current of 100 µA. The full MS scan for both polarities utilized 120,000 resolution with an AGC target of 3e6 and a maximum IT of 100 ms, and the scan range was from 67-1000 *m*/*z*. Tandem MS spectra for both positive and negative mode used a resolution of 15,000, AGC target of 1e5, maximum IT of 50 ms, isolation window of 0.4 m/z, isolation offset of 0.1 m/z, fixed first mass of 50 m/z, and 3-way multiplexed normalized collision energies (nCE) of 10, 35, 80. The minimum AGC target was 1e4 with an intensity threshold of 2e5. All data were acquired in profile mode. All valine data were processed using Thermo XCalibur Qualbrowser for manual inspection and annotation of the resulting spectra and peak heights referring to authentic valine standards and labeled internal standards as described.

RNA Seq

RNA was extracted from cells using the Qiagen RNeasy Kit (Qiagen, 74104) according to the manufacturer's protocol. QIAshredder homogenizer columns (Qiagen, 79654) were used to disrupt the cell lysates. mRNA was purified using the NEBNext poly(A) mRNA Magnetic

Isolation module (New England Biolabs, E7490) in accordance with the manufacturer's protocol. Libraries were prepared using the NEBNext Ultra RNA Library Prep Kit for Illumina (New England Biolabs, E7770), and sequenced on a NextSeq 550 single-end 75 cycles high output with v2.5 chemistry. Reads were adapter and quality trimmed with fastP using default parameters and psuedoaligned to the GCF_003668045.1_CriGri-PICR Chinese hamster genome assembly using kallisto. Differential gene enrichment analysis was performed with in R with DESeq2 and GO enrichment performed and visualized with clusterProfiler against the org.Mm.eg.db database, with further visualization with the pathview, GoSemSim, eulerr packages. Differentially expressed were considered to be statistically significant if their DEseq2 corrected expression was than or equal to the package default of p<= 0.05. GO categories were considered to be statistically significantly regulated if their de/enrichment was calculated as a multiple testing corrected value of p<= 0.05. For mTOR-related genes, all genes present in all GO categories containing the keyword "TOR" were tested for significance with a multiple testing corrected value of p<= 0.05. For ISR genes, a manually curated list of genes consisting of *Eif2ak4, Eif2ak2, Atf4, Ddit3, Asns, Trib3, Nlrp1, Map1lc3b, Atg3, Atg5, Atg7, Atg10, Atg12, Atg16, Becn1, Gabarap, Gabarapl2, Sqstm1, Ddit4, Nupr1, Bcl2l11, Bbc3, Atf5, Pmaip1, Txnip* were tested using a corrected value of p<= 0.05.

Lentiviral packaging

Target plasmid was maintained in and purified from NEB 10-beta electrocompetent *E. coli* (New England Biolabs, C3020K). Lentivirus was packaged by plating $4x10^6$ HEK293T cells on $10cm^2$ and incubating cells overnight at 37°C. Cells were transfected with a plasmid mix consisting of 3.5µg of the target plasmid, 6.0 µg psPAX2 (Addgene, 12260), and 3.0 µg pMD2.G (Addgene, 12259) using Lipofectamine 2000 (ThermoFisher Scientific, 11668019) in accordance with the manufacturer's instructions. Transfected HEK293T cells were incubated for 48 h, before medium was collected, and centrifuged at 200xg for 5 mins. The resulting supernatant was filtered using a 0.45µm filter before infection. CHO cells were plated at 20-30% confluency in and incubated overnight prior to infection. The packaged virus was applied to cells for 24 h before the medium was exchanged for fresh medium. After another 24 h of incubation, the medium was exchanged for fresh medium containing 10µg/ml puromycin for 8 days.

qPCR

gDNA and RNA were extracted from cells using the QIAamp DNA Kit (Qiagen, 51304) the Qiagen RNeasy Kit (Qiagen, 74104), respectively, in accordance with the manufacturer's

protocol. For RNA extraction, QIAshredder homogenizer columns (Qiagen, 79654) were used to disrupt the cell lysates. cDNA was generated from RNA using Invitrogen SuperScript IV Reverse Transcriptase (Invitrogen, 18090200) and oligo(dT) primers. Each qPCR reaction was performed using SYBR Green Master I (Roche, 04707516001) on a Light Cycler 480 (Roche, 05015243001) using the recommended cycling conditions. Primers were designed to amplify amplicons 150-200bp in size.

REFERENCES

1. Payne, S. H. & Loomis, W. F. Retention and loss of amino acid biosynthetic pathways based on analysis of whole-genome sequences. *Eukaryot Cell* **5**, 272–276 (2006).
2. Akashi, H. & Gojobori, T. Metabolic efficiency and amino acid composition in the proteomes of Escherichia coli and Bacillus subtilis. *Proc Natl Acad Sci U S A* **99**, 3695–3700 (2002).
3. Seligmann, H. Cost-minimization of amino acid usage. *J Mol Evol* **56**, 151–161 (2003).
4. Guedes, R. *et al.* Amino acids biosynthesis and nitrogen assimilation pathways: a great genomic deletion during eukaryotes evolution. *BMC Genomics* **12**, S2 (2011).
5. Swire, J. Selection on synthesis cost affects interprotein amino acid usage in all three domains of life. *J Mol Evol* **64**, 558–571 (2007).
6. Zengler, K. & Zaramela, L. S. The social network of microorganisms — how auxotrophies shape complex communities. *Nat Rev Microbiol* **16**, 383–390 (2018).
7. Wilson, A. C. C. & Duncan, R. P. Signatures of host/symbiont genome coevolution in insect nutritional endosymbioses. *Proc Natl Acad Sci U S A* **112**, 10255–10261 (2015).
8. Isaacs, F. J. *et al.* Precise manipulation of chromosomes in vivo enables genome-wide codon replacement. *Science* **333**, 348–353 (2011).
9. Mitchell, L. A. *et al.* Synthesis, debugging, and effects of synthetic chromosome consolidation: synVI and beyond. *Science* **355**, (2017).
10. Fredens, J. *et al.* Total synthesis of Escherichia coli with a recoded genome. *Nature* **569**, 514–518 (2019).
11. Boeke, J. D. *et al.* The Genome Project-Write. *Science* **353**, 126–127 (2016).
12. Heng, B. C., Aubel, D. & Fussenegger, M. Prosthetic gene networks as an alternative to standard pharmacotherapies for metabolic disorders. *Curr Opin Biotechnol* **35**, 37–45 (2015).
13. Tan, X., Letendre, J. H., Collins, J. J. & Wong, W. W. Synthetic biology in the clinic: engineering vaccines, diagnostics, and therapeutics. *Cell* **184**, 881–898 (2021).

14. Kitada, T., DiAndreth, B., Teague, B. & Weiss, R. Programming gene and engineered-cell therapies with synthetic biology. *Science* **359**, (2018).
15. Fischer, S., Handrick, R. & Otte, K. The art of CHO cell engineering: A comprehensive retrospect and future perspectives. *Biotechnol Adv* **33**, 1878–1896 (2015).
16. Szymczak-Workman, A. L., Vignali, K. M. & Vignali, D. A. A. Design and construction of 2A peptide-linked multicistronic vectors. *Cold Spring Harb Protoc* **2012**, 199–204 (2012).
17. O'Gorman, S., Fox, D. T. & Wahl, G. M. Recombinase-mediated gene activation and site-specific integration in mammalian cells. *Science* **251**, 1351–1355 (1991).
18. Hefzi, H. *et al.* A consensus genome-scale reconstruction of Chinese Hamster Ovary cell metabolism. *Cell Syst* **3**, 434-443.e8 (2016).
19. Cunningham, J. A., Liu, A. G., Bengtson, S. & Donoghue, P. C. J. The origin of animals: Can molecular clocks and the fossil record be reconciled? *BioEssays* **39**, 1–12 (2017).
20. Amorim Franco, T. M. & Blanchard, J. S. Bacterial branched-chain amino acid biosynthesis: Structures, mechanisms, and drugability. *Biochemistry* **56**, 5849–5865 (2017).
21. Eagle, H. & Piez, K. THE POPULATION-DEPENDENT REQUIREMENT BY CULTURED MAMMALIAN CELLS FOR METABOLITES WHICH THEY CAN SYNTHESIZE. *J of Exp Med* **116**, 29–43 (1962).
22. Zhenyukh, O. *et al.* High concentration of branched-chain amino acids promotes oxidative stress, inflammation and migration of human peripheral blood mononuclear cells via mTORC1 activation. *Free Rad Biol Med* **104**, 165–177 (2017).
23. Pakos-Zebrucka, K. *et al.* The integrated stress response. *EMBO Rep* **17**, 1374–1395 (2016).
24. Barak, Z., Chipman, D. M. & Gollop, N. Physiological implications of the specificity of acetohydroxy acid synthase isozymes of enteric bacteria. *J Bacteriol* **169**, 3750–3756 (1987).
25. Zhang, Y. *et al.* Expression of threonine-biosynthetic genes in mammalian cells and transgenic mice. *Amino Acids* **46**, 2177–2188 (2014).
26. Rees, W. D. & Hay, S. M. The biosynthesis of threonine by mammalian cells: expression of a complete bacterial biosynthetic pathway in an animal cell. *Biochem J* **309**, 999–1007 (1995).
27. Black, J. B., Perez-Pinera, P. & Gersbach, C. A. Mammalian Synthetic Biology: Engineering Biological Systems. *Annu Rev Biomed Eng* **19**, 249–277 (2017).
28. Gilbert, L. A. *et al.* Genome-scale CRISPR-mediated control of gene repression and activation. *Cell* **159**, 647–661 (2014).

29. Weingarten-Gabbay, S. *et al.* Systematic interrogation of human promoters. *Genome Res* **29**, 171–183 (2019).
30. Lim, A. R., Rathmell, W. K. & Rathmell, J. C. The tumor microenvironment as a metabolic barrier to effector T cells and immunotherapy. *eLife* **9**, e55185.
31. Tan, C. S. H. *et al.* Positive Selection of Tyrosine Loss in Metazoan Evolution. *Science* **325**, 1686–1688 (2009).
32. Dancis, J., Levitz, M. & Westall, R. G. Maple syrup urine disease: branched-chain keto-aciduria. *Pediatrics* **25**, 72–79 (1960).
33. Blau, N., van Spronsen, F. J. & Levy, H. L. Phenylketonuria. *The Lancet* **376**, 1417–1427 (2010).
34. Kemmer, C. *et al.* Self-sufficient control of urate homeostasis in mice by a synthetic circuit. *Nat Biotechnol* **28**, 355–360 (2010).
35. Ye, H. *et al.* Pharmaceutically controlled designer circuit for the treatment of the metabolic syndrome. *Proc Natl Acad Sci U S A* **110**, 141–146 (2013).
36. Pan, X. *et al.* dSLAM analysis of genome-wide genetic interactions in Saccharomyces cerevisiae. *Methods* **41**, 206–221 (2007).
37. Pacold, M. E. *et al.* A PHGDH inhibitor reveals coordination of serine synthesis and one-carbon unit fate. *Nat Chem Biol* **12**, 452–458 (2016).

Acknowledgements

We would like to thank the members of the Boeke and Wang labs for comments and discussion on the work and manuscript. RMM additionally thanks personal support from Xiaoyu Weng.

Funding

Defense Advanced Research Projects Agency HR0011-17-2-0041 (HHW, JDB)
National Institutes of Health / National Human Genome Research Institute RM1 HG009491 (JDB)
National Science Foundation MCB-1453219 (HHW)
Burroughs Wellcome Fund PATH1016691 (HHW)
Irma T. Hirschl Trust (HHW)
Dean's Fellowship from the Graduate School of Arts and Sciences of Columbia University (RMM)

Competing interests

Jef D. Boeke is a Founder and Director of CDI Labs, Inc., a Founder of Neochromosome, Inc, a Founder and SAB member of ReOpen Diagnostics, and serves or served on the Scientific Advisory Board of the following: Sangamo, Inc., Modern Meadow, Inc., Rome Therapeutics Inc., Sample6, Inc., Tessera Therapeutics, Inc. and the Wyss Institute.

Data and availability

Sequencing data generated for this study is deposited in the NCBI SRA at accession number PRJNA742028. Source data files have been provided for Figure 1 – figure supplement 1, Figure 1 – figure supplement 2D, Figure 2, Figure 2 – figure supplement 3, Figure 2 – figure supplement 4B, Figure 2 – figure supplement 5, Figure 2 – figure supplement 6, Figure 3, and Figure 3 – figure supplement 1, Figure 4, Figure 4 – figure supplement 1, Figure 5, and Figure 5 – figure supplement 1.

FIGURES

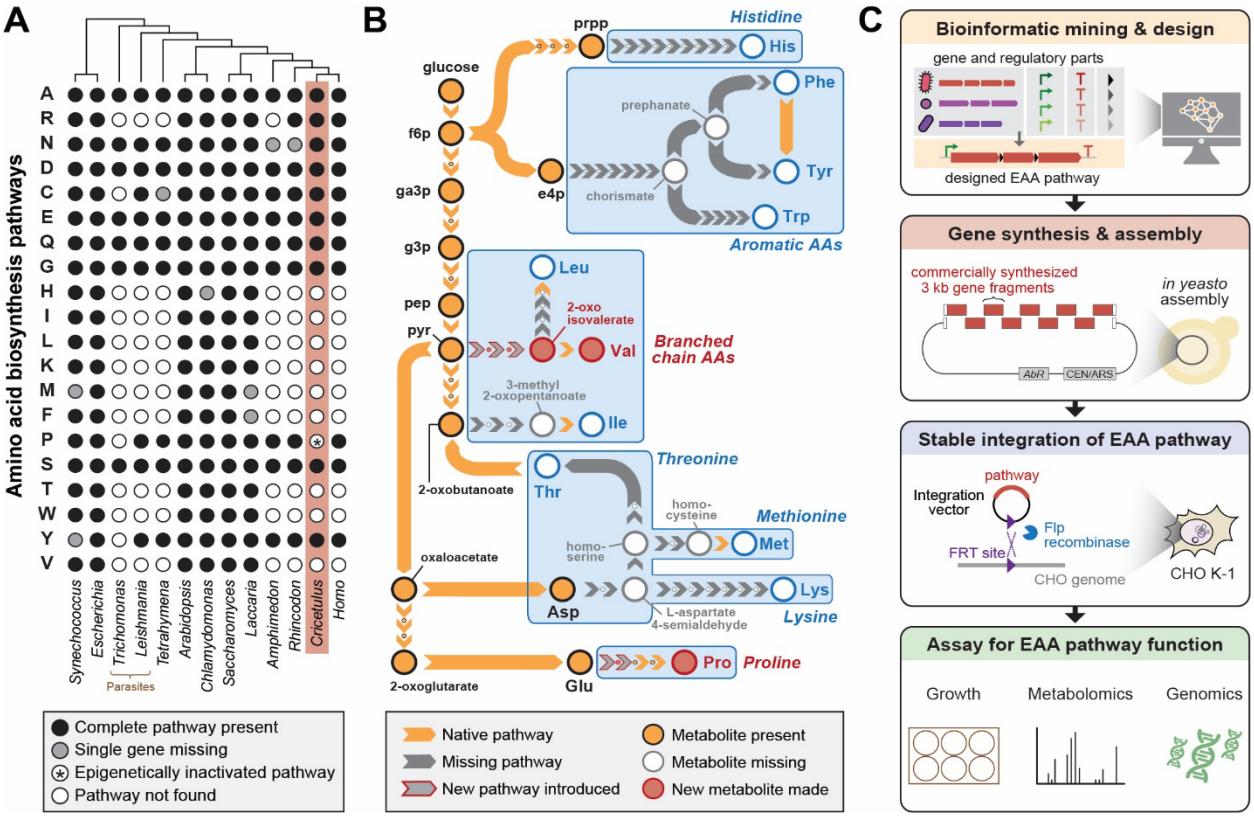

Figure 1. Engineering Essential Amino Acid (EAA) biosynthesis in metazoan cells.
(A) Presence of amino acid biosynthesis pathways across representative diverse organisms on Earth. **(B)** Schematic of EAA biosynthesis pathway steps that require engineering in mammalian cells to enable complete amino acid prototrophy if imported from *E. coli*. Proline and Valine pathways shown in this work are highlighted in red. **(C)** Workflow diagram of a synthetic genomics approach involving pathway design, construction, integration and testing towards mammalian EAA restoration.

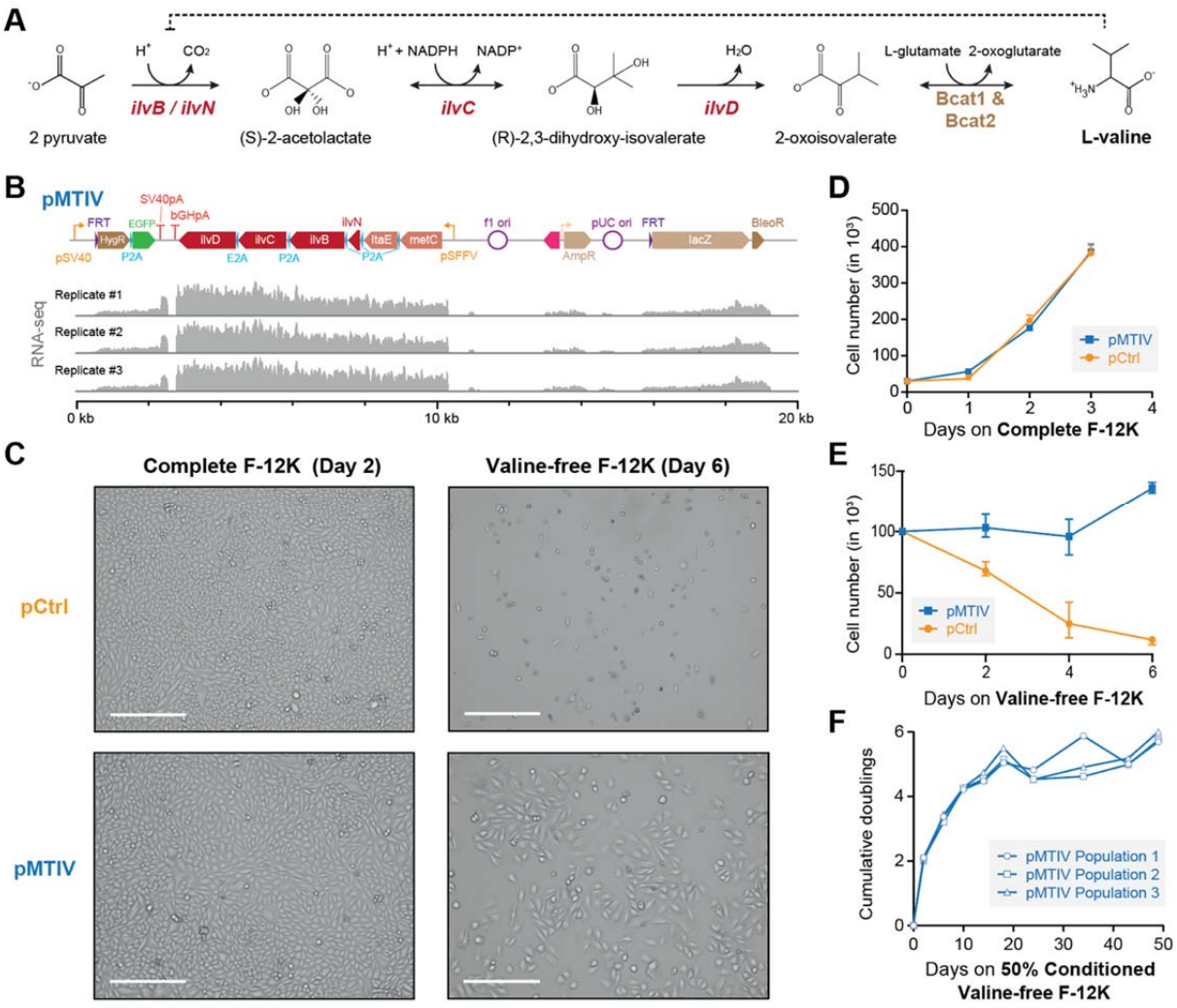

Figure 2. Restoration of a Valine biosynthesis pathway in CHO-K1 cells.

(A) Three enzymatic steps encoded by *E. coli* genes *ilvN* (regulatory subunit, acetolactate synthase), *ilvB* (catalytic subunit, acetolactate synthase), *ilvC* (ketol-acid reductoisomerase), and *ilvD* (dihydroxy-acid dehydratase) are required for valine biosynthesis in CHO-K1 cells. **(B)** Schematic of pMTIV construct after genomic integration and RNA-seq read coverage showing successful incorporation and active transcription. **(C)** Microscopy images of CHO-K1 cells with integrated pCtrl or pMTIV constructs in complete F-12K medium after 2 days or valine-free F-12K medium after 6 days. Scale bar represents 300µm. **(D)** Growth curve of CHO-K1 cells with pCtrl or pMTIV in complete F-12K medium **(Figure 2-source data 1)**. Day 0 indicates number of seeded cells. Triplicate values are plotted. **(E)** Growth curve of CHO-K1 cells with pCtrl or pMTIV in valine-free F-12K medium **(Figure 2-source data 1)**. Day 0 indicates number of seeded cells. Triplicate values are plotted. **(F)** CHO-K1 with pMTIV cultured over 9 passages in 50% conditioned valine-free F-12K medium **(Figure 2-source data 1)**.

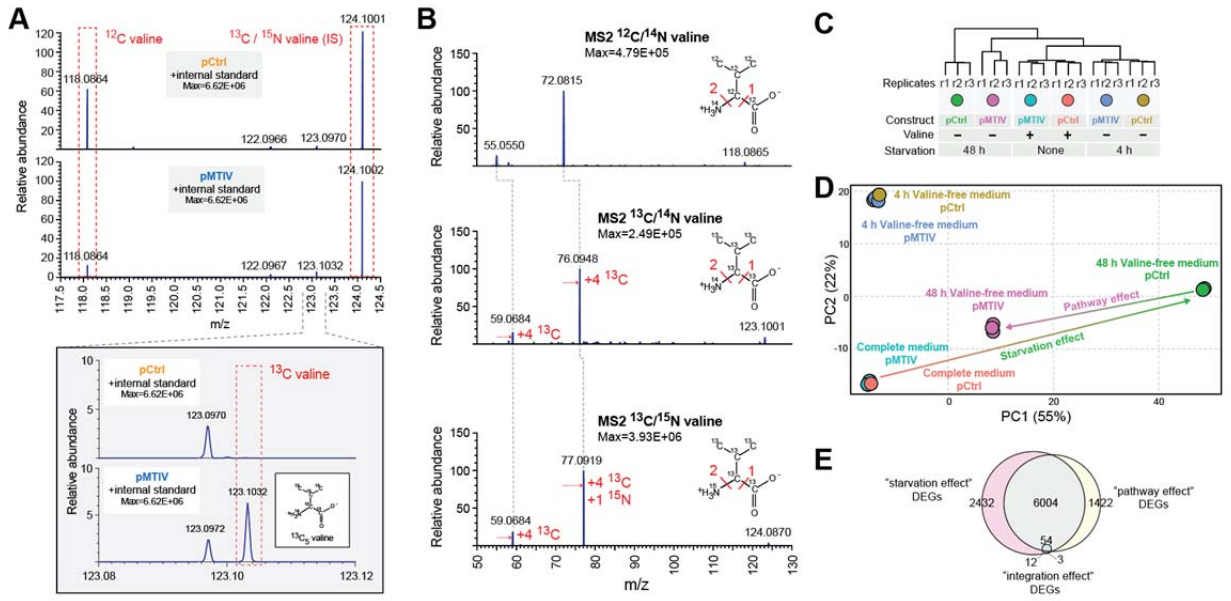

Figure 3. Heavy-carbon validation of endogenous valine production and transcriptomic signatures associated with rescue of nutritional starvation

(A) Mass spectra showing an MS1 peak corresponding to the expected *m*/*z* for ^{13}C-valine when pMTIV cells were grown on valine-free RPMI medium supplemented with ^{13}C-glucose and ^{13}C-pyruvate, indicating autogenous production of intracellular valine **(Figure 3-source data 1)**. **(B)** MS2 performed on peaks extracted from pMTIV sample, which corresponded to *m*/*z* values expected for ^{12}C-valine, ^{13}C-valine and internal standard ^{13}C/^{15}N-valine. MS2 fragmentation patterns for each of these metabolites matched expectations **(Figure 3-source data 1)**. **(C)** RNA-seq dendrogram of pCtrl cells and pMTIV cells grown on complete F-12K medium or starved of valine for 4 or 48 hours. **(D)** PCA space depiction of pCtrl cells and pMTIV cells grown on complete F-12K medium, or starved of valine for 4 or 48 hours. **(E)** Overlap between Differently Expressed Genes (DEGs) comparing pCtrl cells cultured in valine-free F-12K medium to pCtrl cells cultured in complete F-12K medium (the “starvation effect”), pCtrl cells and pMTIV cells after 48 hours starvation on valine-free F-12K medium (the “pathway effect”), and pCtrl cells and pMTIV cells grown on complete F-12K medium (the “integration effect”).

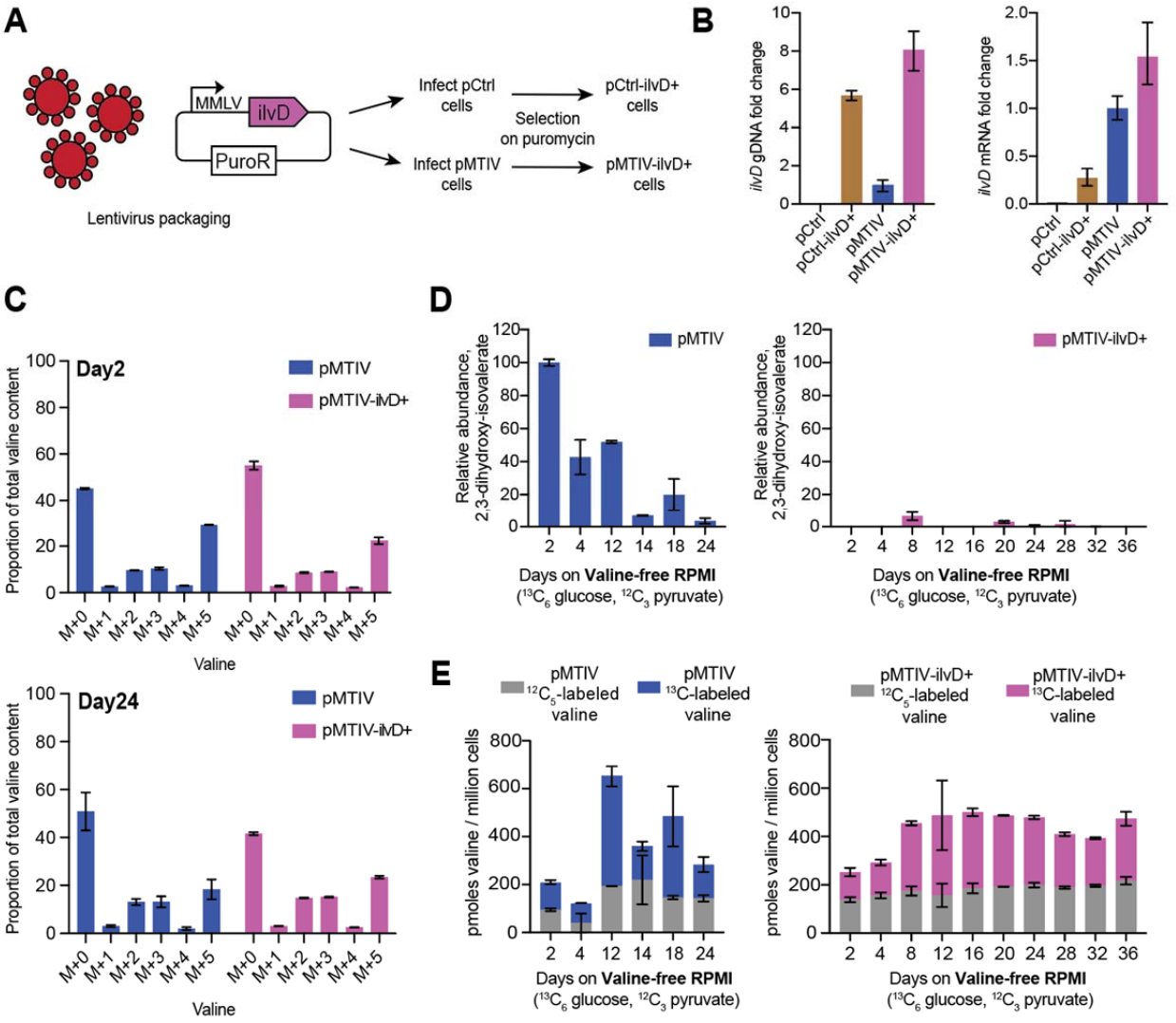

Figure 4. Optimization of prototrophic functionality reduces pathway bottlenecking and stabilizes valine availability at late time points in valine-free conditions

(A) Infection of pCtrl and pMTIV cells using a lentivirus carrying extra copies of *ilvD* led to the generation of the pCtrl-ilvD+ and pMTIV-ilvD+ cell lines. **(B)** *ilvD* qPCR on gDNA and cDNA from each cell line **(Figure 4-source data 1)**. Fold change levels were relativized to pMTIV. cDNA was reverse transcribed using oligo(dT) primers from RNA templates collected from each cell line. **(C)** ^{13}C-labeling of valine in pMTIV and pMTIV-ilvD+ samples collected on day 2 and day 24 of culture in unconditioned, reduced-isoleucine (0.06 mM), valine-free RPMI medium containing $^{13}C_6$-glucose with 2 mM ^{12}C-sodium pyruvate spiked-in on plates coated with 0.1% gelatin **(Figure 4-source data 1)**. Duplicate values are plotted. **(D)** Relative abundance of pathway intermediate 2,3-dihydroxy-isovalerate in pMTIV and pMTIV-ilvD+ cells cultured as in (C) **(Figure 4-source data 1)**. Duplicate values are plotted. **(E)** Molar concentration of valine in

638 pMTIV and pMTIV-ilvD+ cells cultured as in (C) **(Figure 4-source data 1)**. ^{12}C-labeled refers to
639 valine carrying ^{12}C exclusively while ^{13}C-labeled refers to valine carrying at least one ^{13}C.
640 Duplicate values are plotted.
641

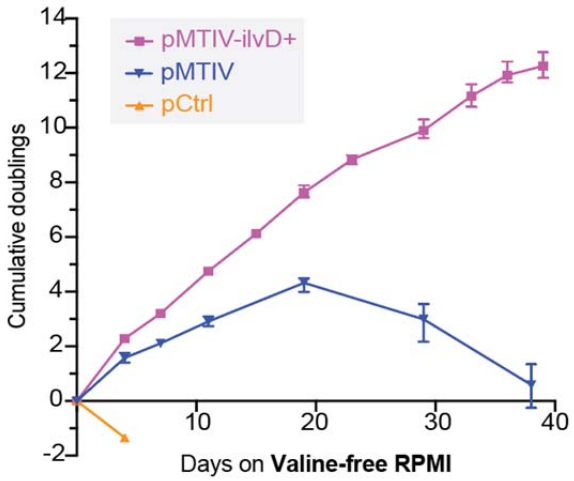

Figure 5. Optimized prototrophic cells double every 3.2 days in unconditioned valine-free RPMI medium over 39 days.

Population doubling level of pCtrl, pMTIV, pMTIV-ilvD+ cells cultured in unconditioned, reduced-isoleucine, valine-free RPMI medium containing 2 mM sodium pyruvate **(Figure 5-source data 1)**. Plates were not coated with gelatin. Triplicate values are plotted.

FIGURE SUPPLEMENTS

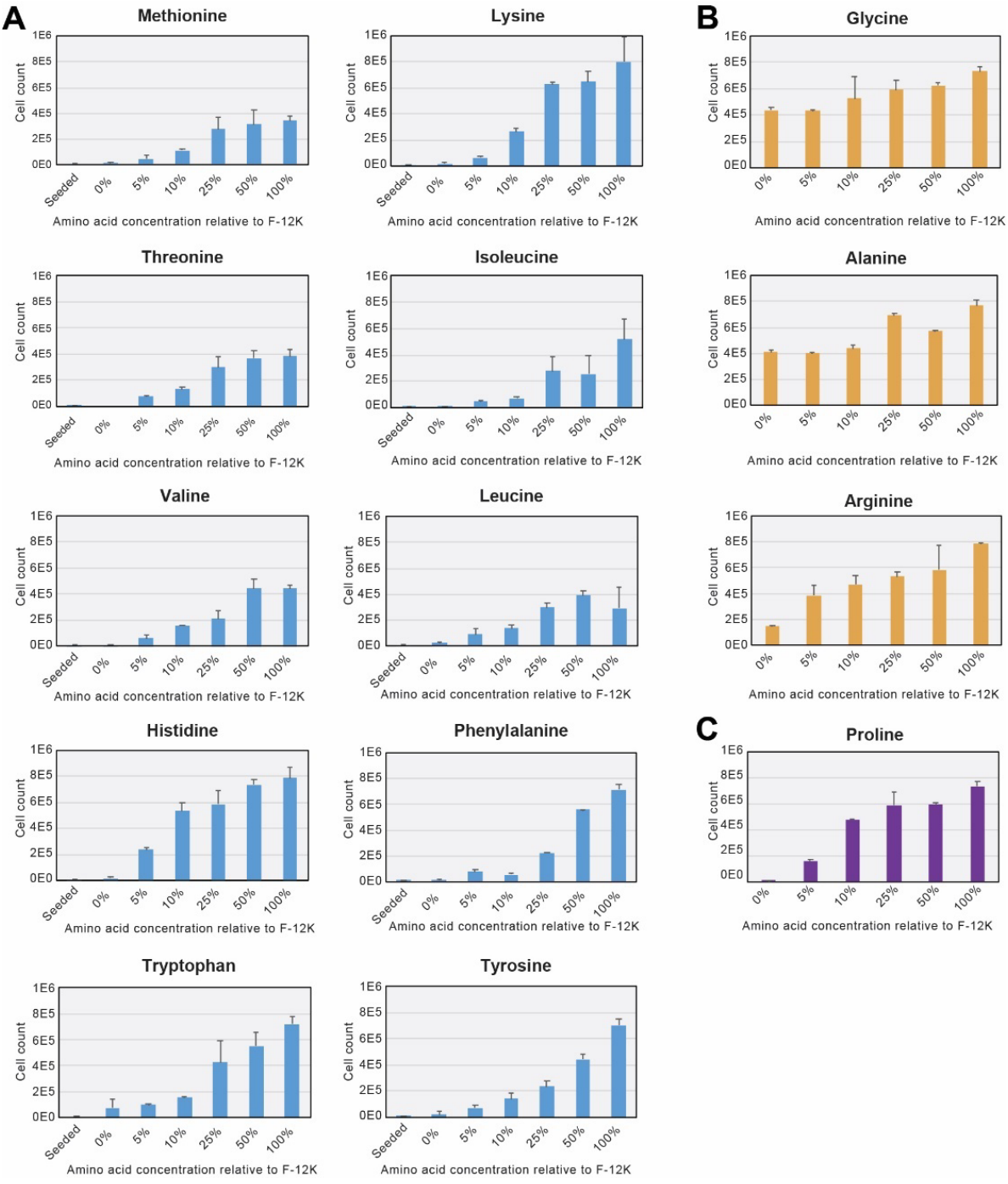

Figure 1 – figure supplement 1. Amino acid dropout growth assays in CHO-K1.

(A) Growth assays on CHO-K1 cells seeded into media with reduced or omitted essential amino acids **(Figure 1-figure supplement 1-source data 1)**. Percentages represent the relative media amino acid concentration compared to standard F-12K medium. 100% corresponds to

0.02 mM (Trp), 0.05 mM (Tyr), 0.06 mM (Ile, Met, Phe), 0.2 mM (Ala, Asn, Asp, Glu, Gly, Leu, Ser, Thr, Val), 0.22 mM (His), 0.4 mM (Cys, Lys), 0.6 mM (Pro), and 2 mM (Arg, Gln), respectively. Error bars show standard deviation of three replicates. **(B)** CHO-K1 cells grow with minimal defects in F-12K medium lacking glycine and alanine, but are more sensitive to arginine starvation **(Figure 1-figure supplement 1-source data 1)**. **(C)** CHO cells do not grow without exogenous proline, confirming the known epigenetic proline auxotrophy found in this cell line **(Figure 1-figure supplement 1-source data 1)**. Error bars show standard deviation of three replicates.

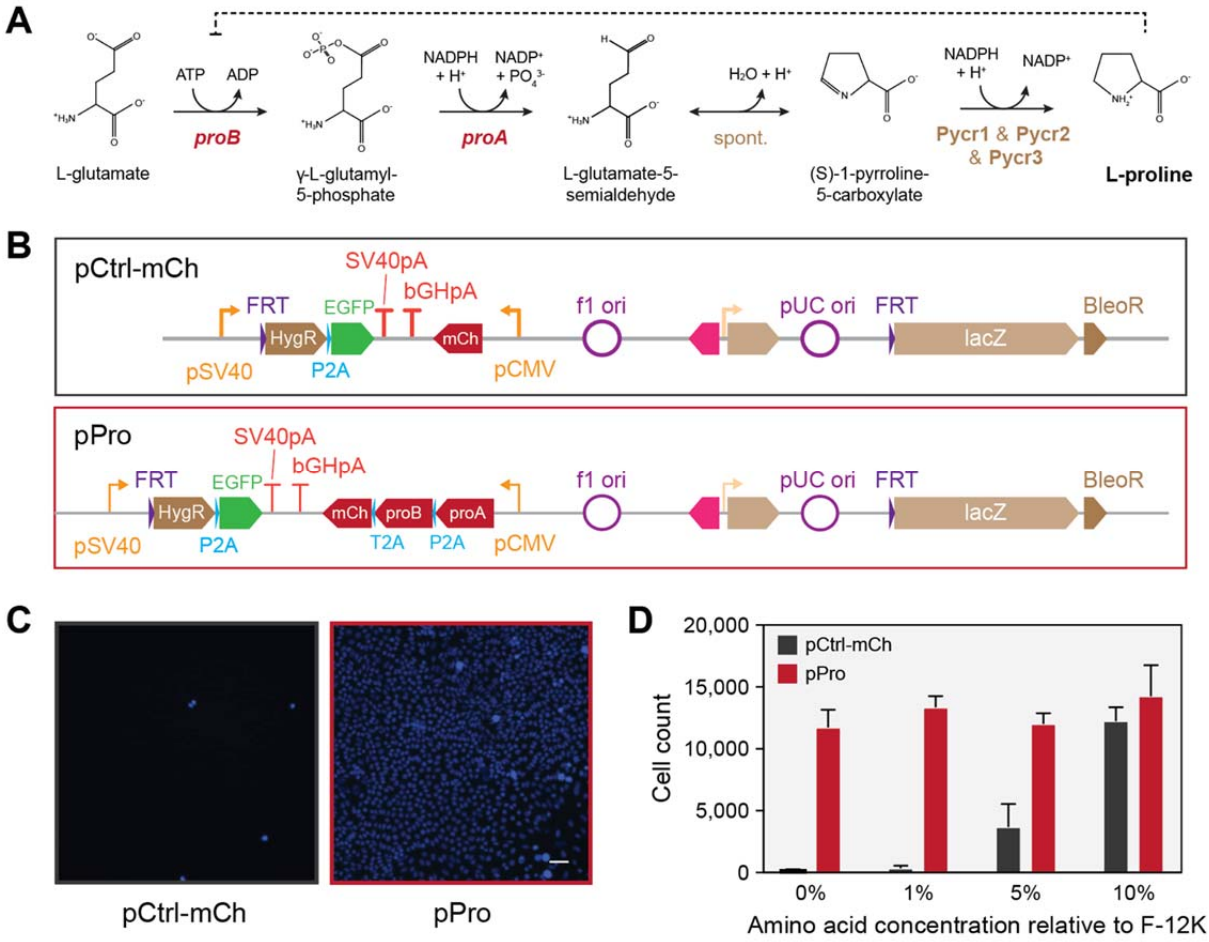

Figure 1 – figure supplement 2. Imported bacterial genes rescue CHO epigenetic proline auxotrophy

(A) Proline biosynthetic pathway from glutamate. **(B)** Schematic representation of two constructs to test bacterial gene rescue of CHO-K1 auxotrophy, one expressing the *E. coli proA* and *proB* genes, encoding glutamate-5-semialdehyde dehydrogenase and glutamate-5-kinase, respectively (pPro), and a control construct expressing only mCherry (pCtrl-mCh)**.** Constructs are shown as they appear following integration into the Flp-In CHO line. **(C)** Hoechst 33348 live nuclei microscopy shows cells expressing the pPro construct grow in the absence of proline and appear healthy. Scale bar represents 50 μm and is shared across images **(D)** Growth assay of cells seeded into proline-free F-12K medium and grown for 5 days **(Figure 1-figure supplement 2-source data 1)**. The bacterial gene pPro pathway resulted in robust growth recovery in proline-free medium. Error bars show standard deviation of three replicates.

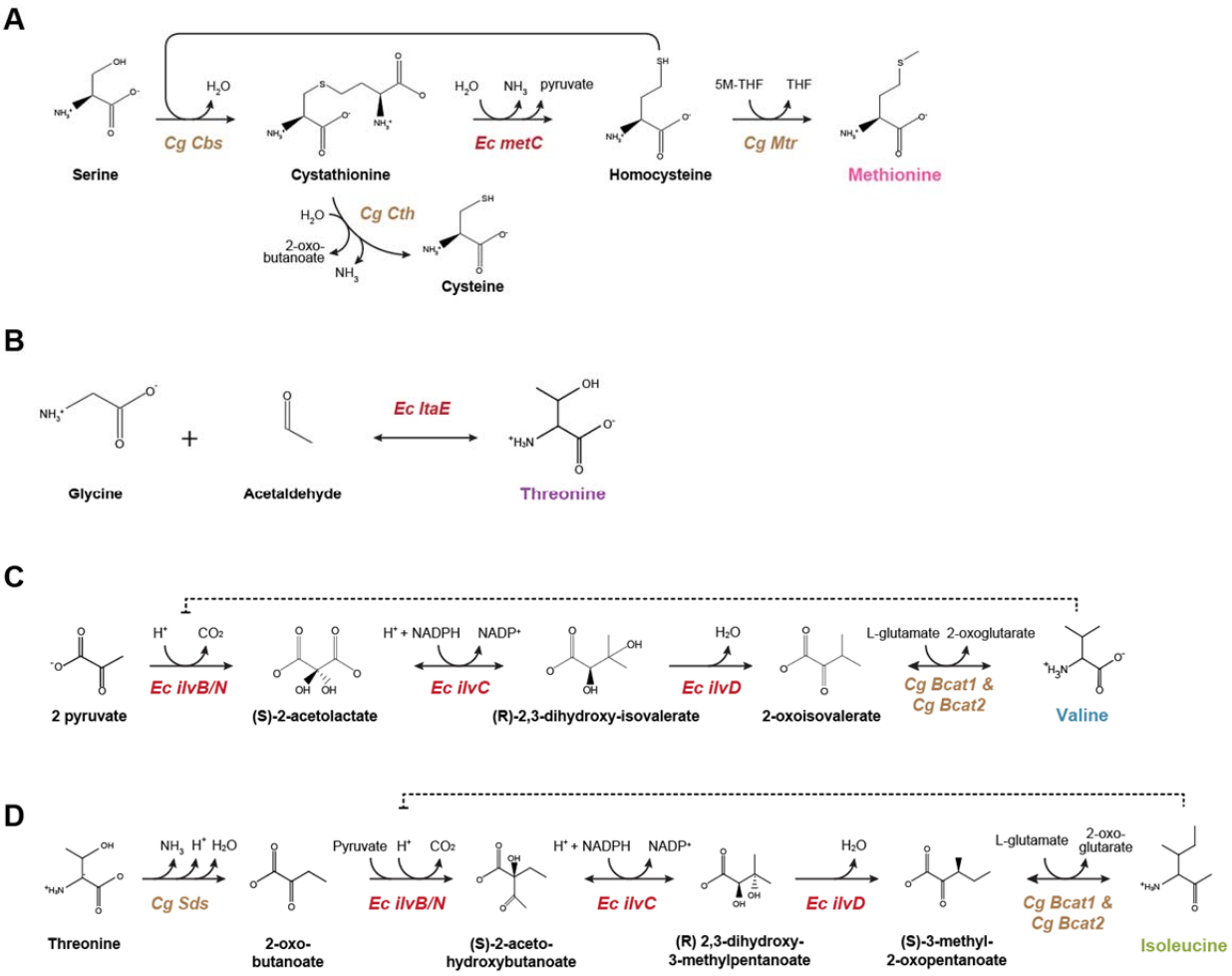

677

678 **Figure 2 – figure supplement 1. Schematic outlines of the MTIV pathways.**

679 **(A)** Pathway for methionine biosynthesis**. (B)** Pathway for threonine biosynthesis**.** Note the
680 shared multifunctional enzymes in **(C)** and **(D)** responsible for both isoleucine and valine
681 production. In all panels "*Ec*" refers to *E. coli,* and *"Cg"* to *C. griseus*, the native CHO parental
682 organism. Red genes indicate steps missing in CHO metabolism.

683

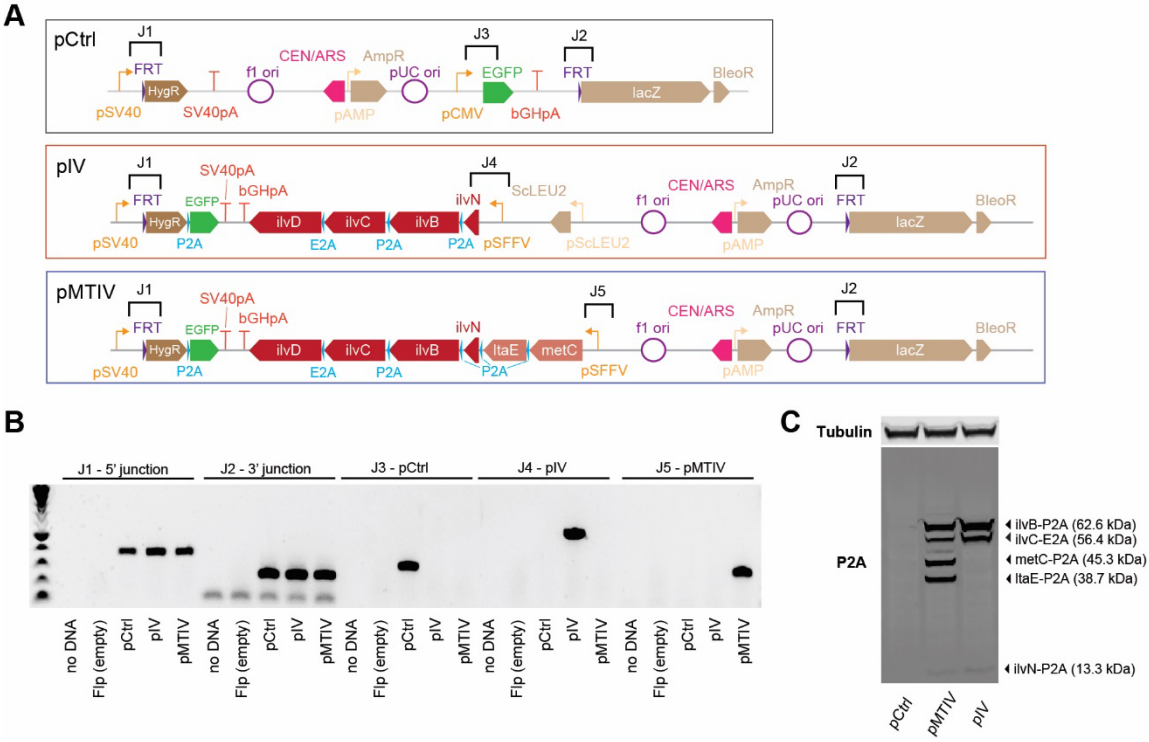

Figure 2 – figure supplement 2. Confirmation of BCAA biosynthetic construct integration and 2A peptide processing by PCR and Western blot

(A) Construct were designed with PCR landing pads flanking fragment junctions for rapid screening during construct assembly *in yeasto,* shown above construct diagrams with brackets. **(B)** PCRs across these junctions confirm correct assembly of the control, pMTIV, and pIV constructs **(Figure 2-figure supplement 2-source data 1)**. **(C)** Immunoblotting against P2A peptides in pMTIV and pIV cells confirms 2A peptides are processed as expected **(Figure 2-figure supplement 2-source data 2)**. Note that *ilvD* (65.5 kDa) is not detectable because it lacks a terminal P2A tag.

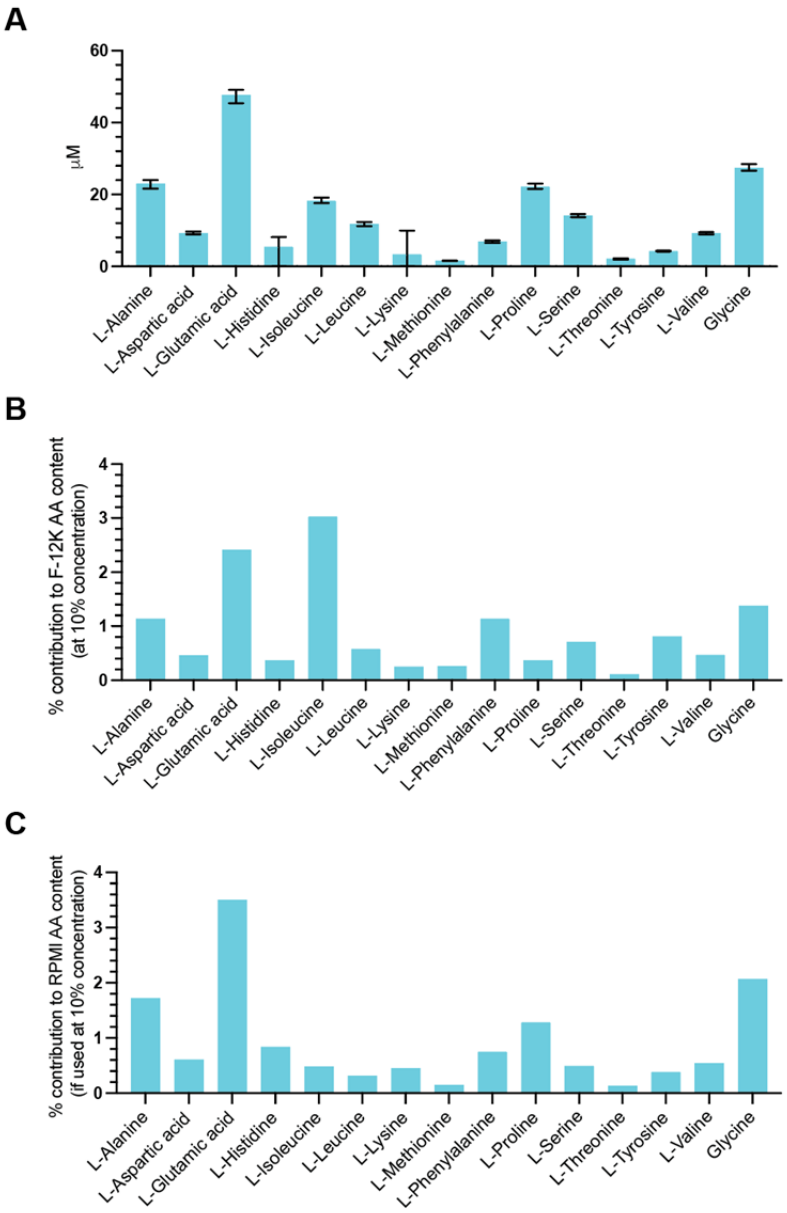

Figure 2 – figure supplement 3. Amino acid content in dialyzed fetal bovine serum. **(A)** Concentration of 15 different proteinogenic amino acids in dialyzed fetal bovine serum. Triplicate values are plotted **(Figure 2-figure supplement 3-source data 1)**. **(B)** The amino acid contribution of dialyzed fetal bovine serum to non-supplemented F-12K medium when supplemented at 10% concentration. **(C)** The amino acid contribution of dialyzed fetal bovine serum to non-supplemented RPMI medium when supplemented at 10% concentration.

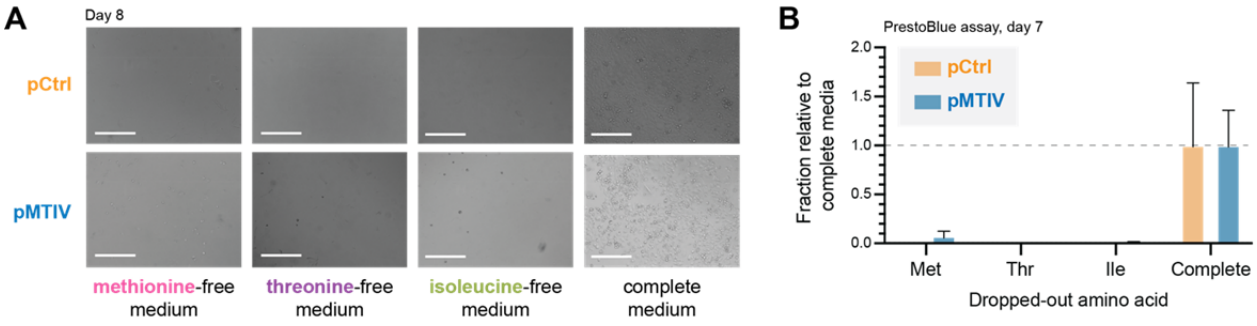

Figure 2 – figure supplement 4. Lack of rescue of methionine, threonine and isoleucine auxotrophy by pMTIV construct in CHO-K1 cells.

(A) Phase-contrast images of cells carrying either pMTIV and pCtrl constructs after 8 days growth on EAA-free F-12K media (three leftmost panels) or complete F-12K medium (rightmost panel). Scale bar represents 300μm. **(B**) PrestoBlue™ cell viability assay of growth on EAA-free or complete media after 7 days' growth **(Figure 2-figure supplement 4-source data 1)**. Error bars show standard deviation of three replicates.

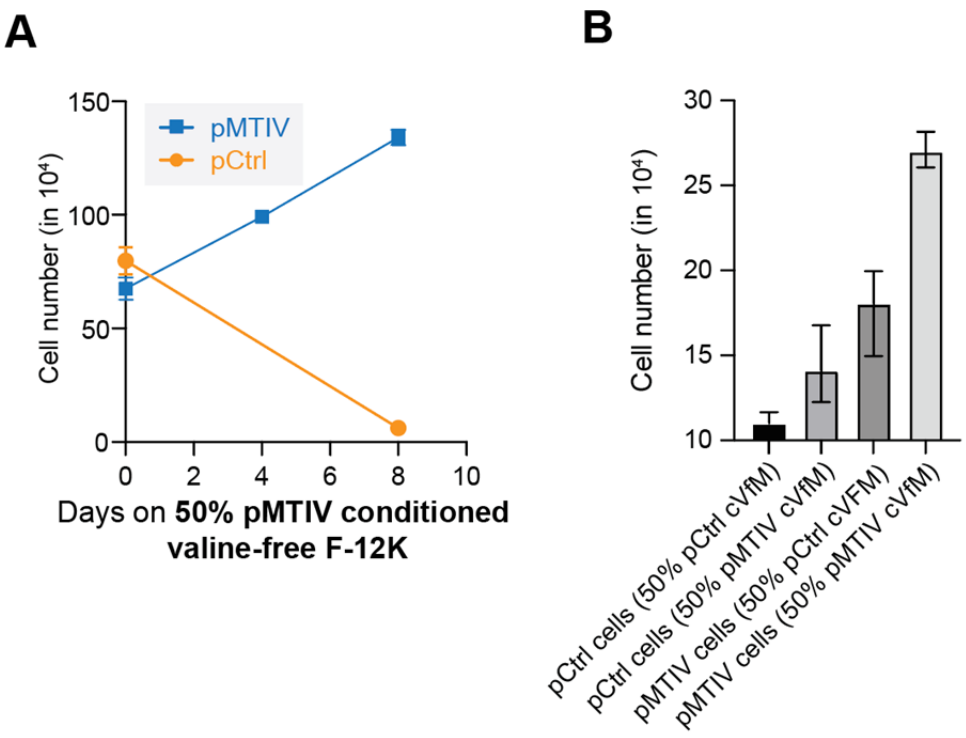

Figure 2 - figure supplement 5. Growth behaviors on conditioned valine-free F-12K medium.

(A) Growth and death of pMTIV and pCtrl cells on 50% conditioned valine-free F-12K medium. Triplicate values are plotted **(Figure 2-figure supplement 5-source data 1)**. **(B)** Comparison of pCtrl and pMTIV cells grown on 50% conditioned valine-free F-12K medium using medium conditioned by pCtrl (50% pCtrl cVfM) and medium conditioned by pMTIV cells (50% pMTIV cVfM) as indicated **(Figure 2-figure supplement 5-source data 1)**. Triplicate values are plotted.

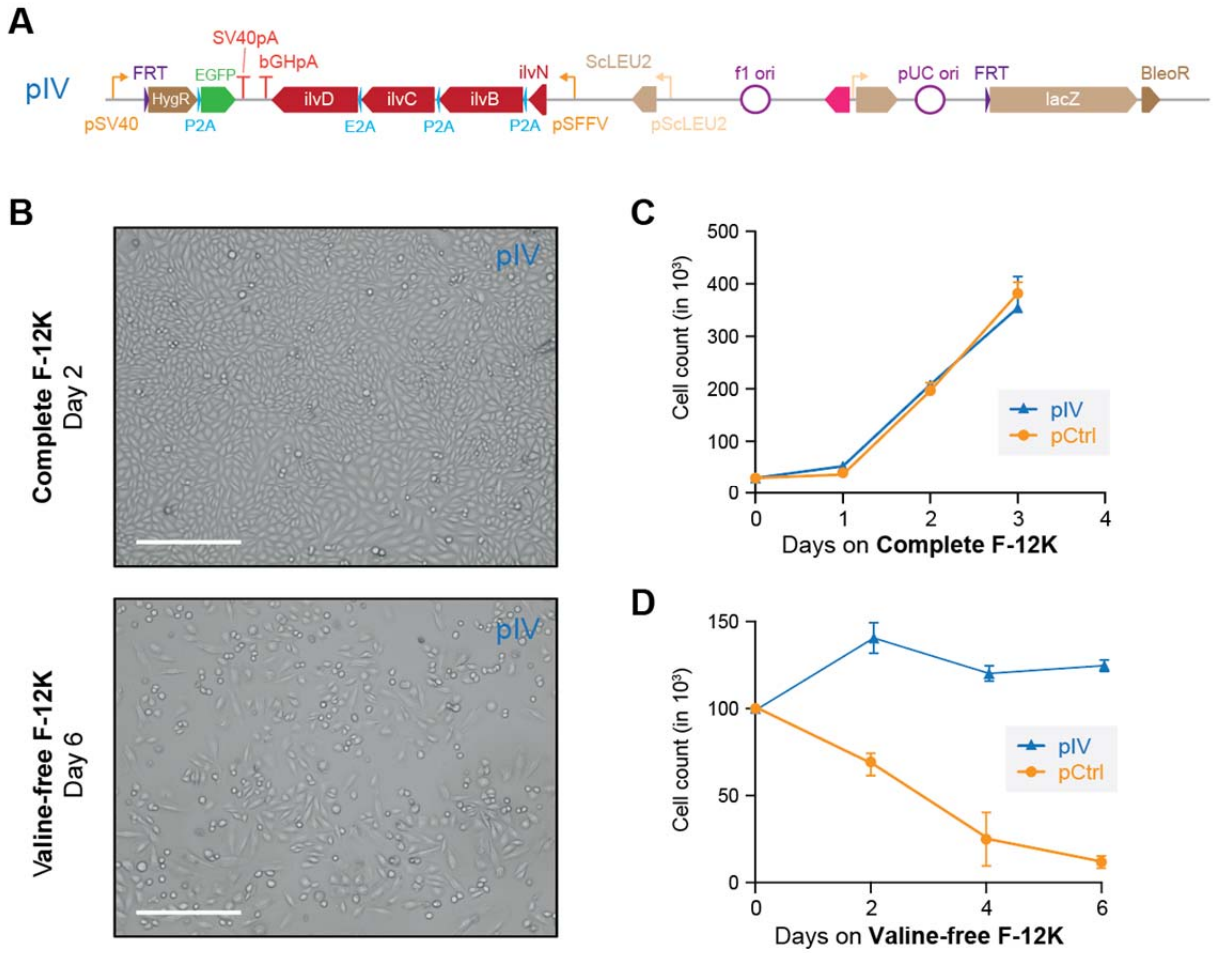

Figure 2 – figure supplement 6. The pIV construct rescues valine auxotrophy

(A) The minimized four-gene construct pIV lacking *ltaE*-encoded L-threonine aldoase and *metC*-encoded cystathionine-ß-lyase after integration into the CHO genome. **(B)** Microscopy of pIV cells in both complete and valine-free F-12K medium. The pIV constructs rescue cellular morphology in valine-free F-12K medium. Scale bar represents 300µm. **(C)** Growth of pIV cells in complete F-12K medium **(Figure 2-figure supplement 6-source data 1)**. Error bars show standard deviation of three replicates. **(D)** Live cell counting of pIV cells grown on valine-free F-12K **(Figure 2-figure supplement 6-source data 1)**. Triplicate values are plotted.

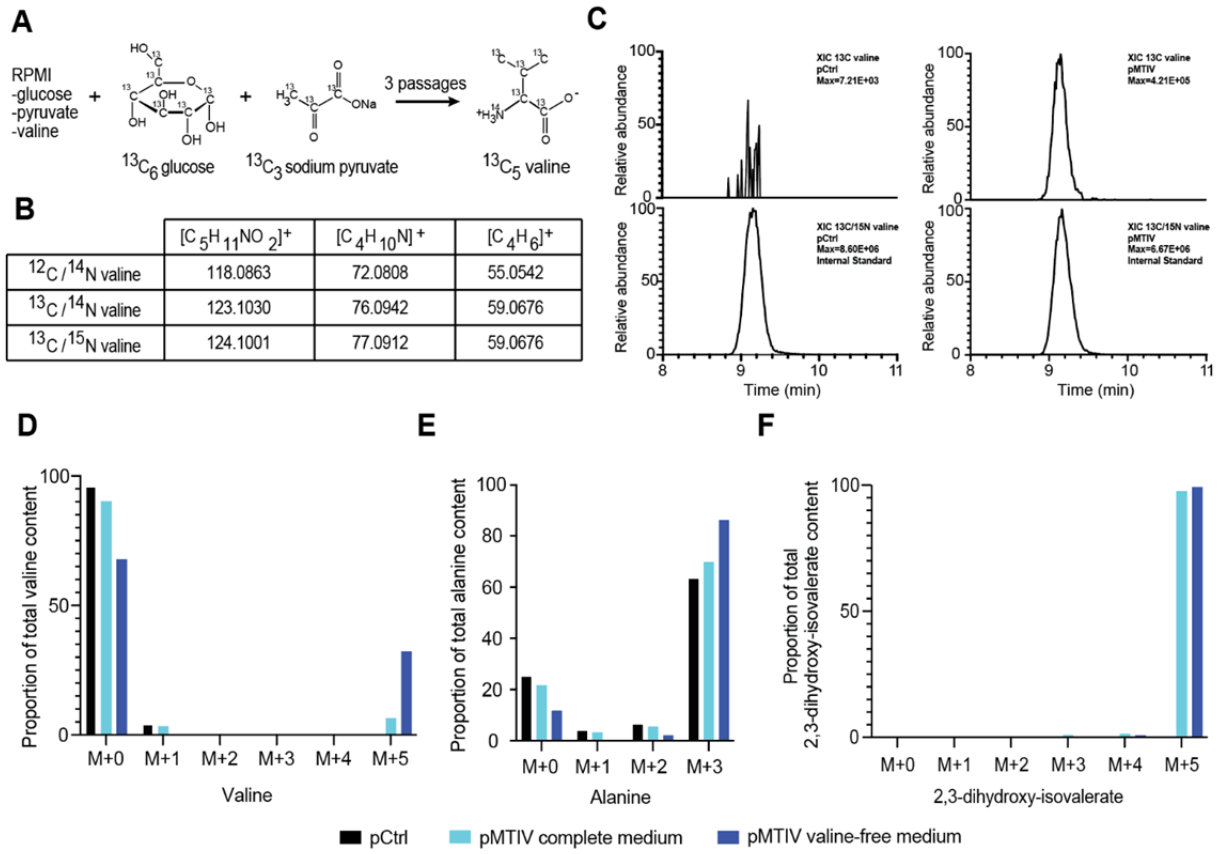

	$[C_5H_{11}NO_2]^+$	$[C_4H_{10}N]^+$	$[C_4H_6]^+$
$^{12}C/^{14}N$ valine	118.0863	72.0808	55.0542
$^{13}C/^{14}N$ valine	123.1030	76.0942	59.0676
$^{13}C/^{15}N$ valine	124.1001	77.0912	59.0676

Figure 3 – figure supplement 1. Heavy-labeled metabolomics confirms endogenous valine production

(A) Schematic outline of the ^{13}C-labeling strategy for detection of biosynthesized valine. **(B)** Expected *m/z* ratios for ^{12}C-valine, ^{13}C-valine, and spiked-in internal standard $^{13}C/^{15}N$-valine in unfragmented and fragmented states. **(C)** Extracted ion chromatography shows that the presumed ^{13}C-valine found in pMTIV cells runs similarly to spiked-in internal standard $^{13}C/^{15}N$-valine, further confirming that ^{13}C-valine is produced in pMTIV cells **(Figure 3-figure supplement 1-source data 1)**. The presence of ^{13}C-valine is specific to pMTIV cells and absent from control cells. **(D)**. In theory, partial ^{13}C-labeling of valine is possible if just one of the two pyruvate substrates is ^{13}C-labeled. Partially ^{13}C-labeled ($^{13}C_2$, $^{13}C_3$, $^{13}C_4$) valine species were below the level of detection. Therefore, the proportion of $^{13}C_5$-valine relative to total valine abundance within the cell can serve as a proxy for the degree to which intracellular valine biosynthesis is meeting cellular valine demands. The lesser occurrence of $^{13}C_1$-valine can be explained by the natural abundance of ^{13}C. 32.2% of total valine abundance in pMTIV cells cultured in valine-free RPMI medium was $^{13}C_5$-labeled whereas the corresponding proportion for pMTIV cells cultured in complete RPMI medium was 6.4% **(Figure 3-figure supplement 1-source data 1). (E)** Non-essential amino acid alanine is biosynthesized from pyruvate and is

not found in RPMI medium. Alanine can thus serve a proxy for proteome turnover assuming similar usage rates for alanine and valine. 86.1% of alanine was $^{13}C_3$-alanine in pMTIV cells cultured in valine-free RPMI medium **(Figure 3-figure supplement 1-source data 1)**. **(F)** ^{13}C-labeled pathway intermediate 2,3-dihydroxy-isovalerate was detected in pMTIV cells cultured in complete and in valine-free RPMI conditions **(Figure 3-figure supplement 1-source data 1)**.

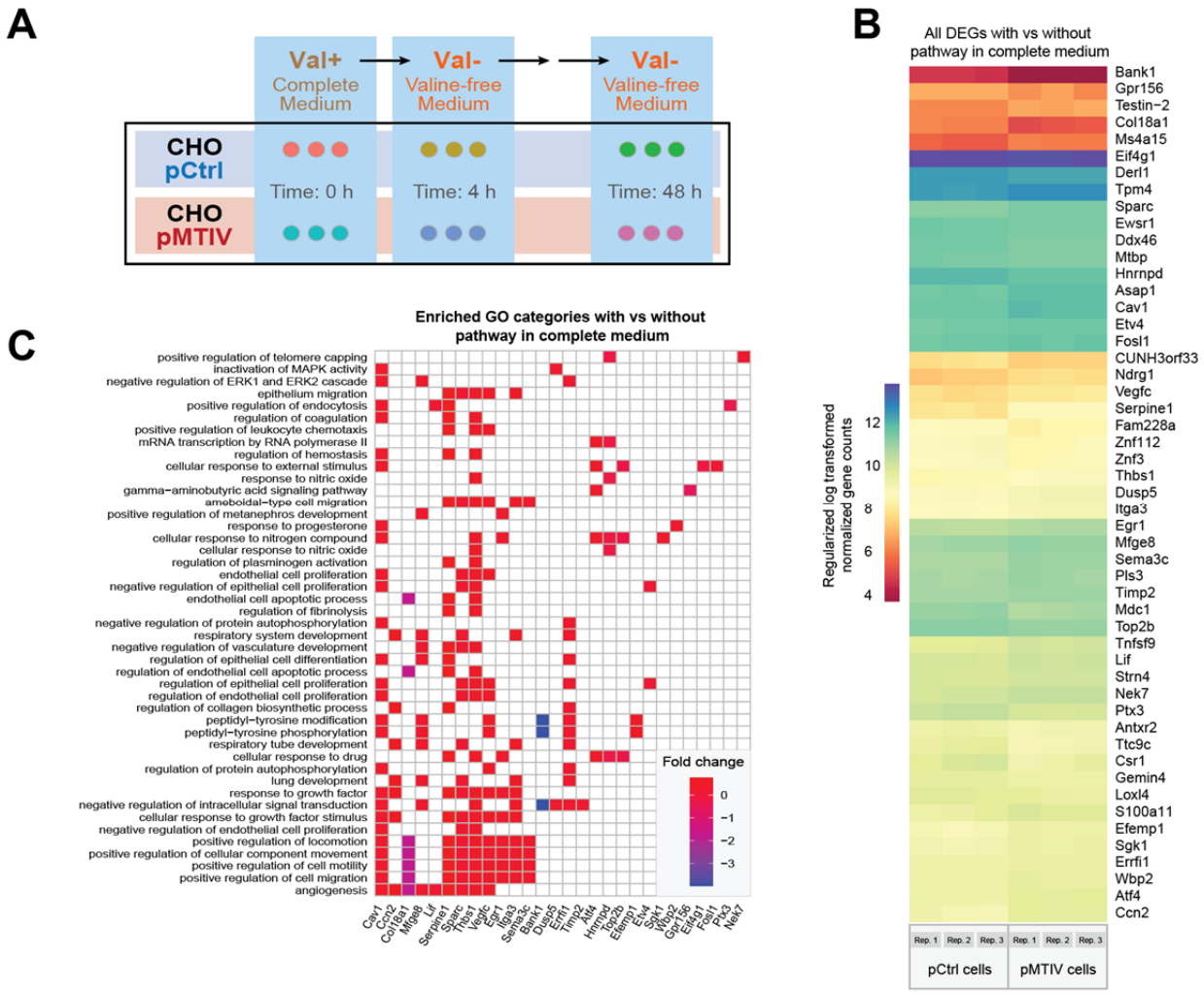

761

762 **Figure 3 – figure supplement 2. Transcriptomic analysis of pMTIV pathway effect in**
763 **complete F-12K medium.**

764 **(A)** Schematic representation of the starvation regimen applied prior to collecting samples for
765 transcriptomic analysis. **(B)** Regularized log fold changes in expression across the 51
766 differentially expressed genes when comparing pMTIV cells to pCtrl cells grown in complete
767 medium. Values from three replicates are plotted side-by-side in each column. **(C)** GO category
768 enrichment among the 51 differentially expressed genes.

769

770

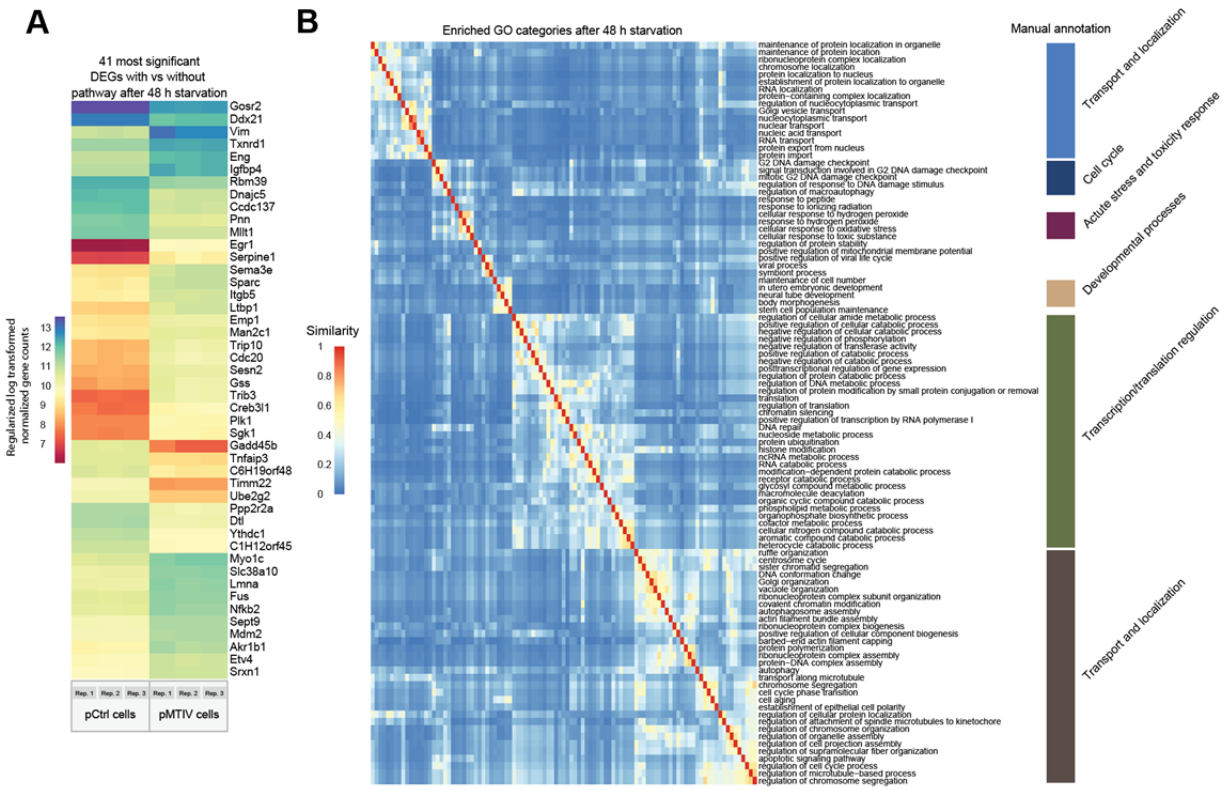

Figure 3 – figure supplement 3. Transcriptomic analysis of pMTIV pathway effect in valine-free F-12K medium.

(A) Regularized log transformed expression of the 50 most significant differentially expressed genes when comparing pMTIV cells to pCtrl cells after 48 h in valine-free F-12K medium. Values from three replicates are plotted side-by-side in each column. **(B)** GO category enrichment among these genes, clustered and colored using a GO ontology distance metric, and manually grouped into larger supercategories, on the right.

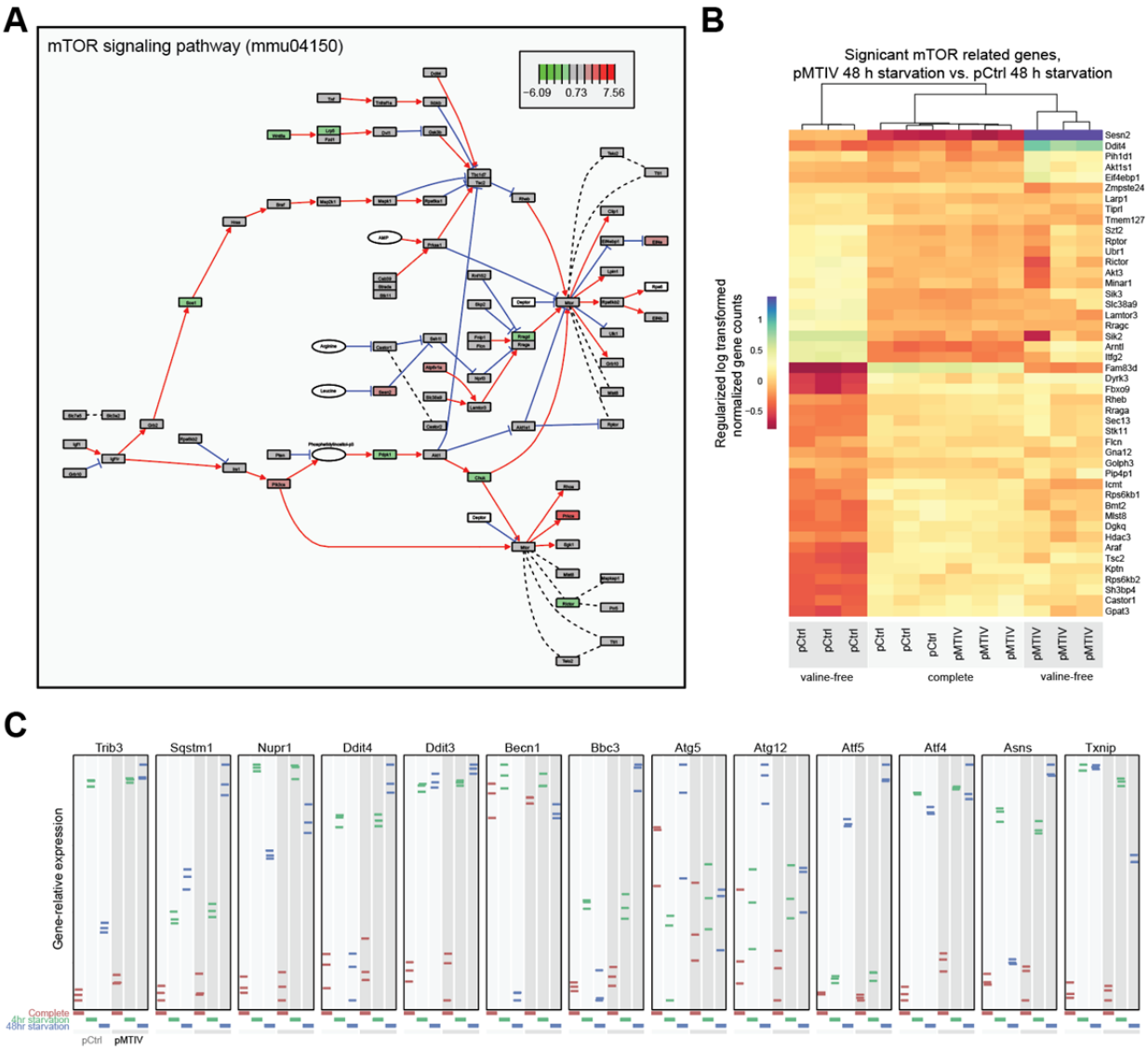

Figure 3 – figure supplement 4. Transcriptomic analysis of pMTIV pathway effect on mTOR and the integrated stress response.

(A) KEGG representation of the mouse mTOR pathway showing individual node gene up/down regulation. **(B)** Significantly differently expressed mTOR-related genes after 48 h valine starvation in pMTIV cells. **(C)** Significantly differently expressed Integrated Stress Response-related genes after 48 h valine starvation in pMTIV cells.

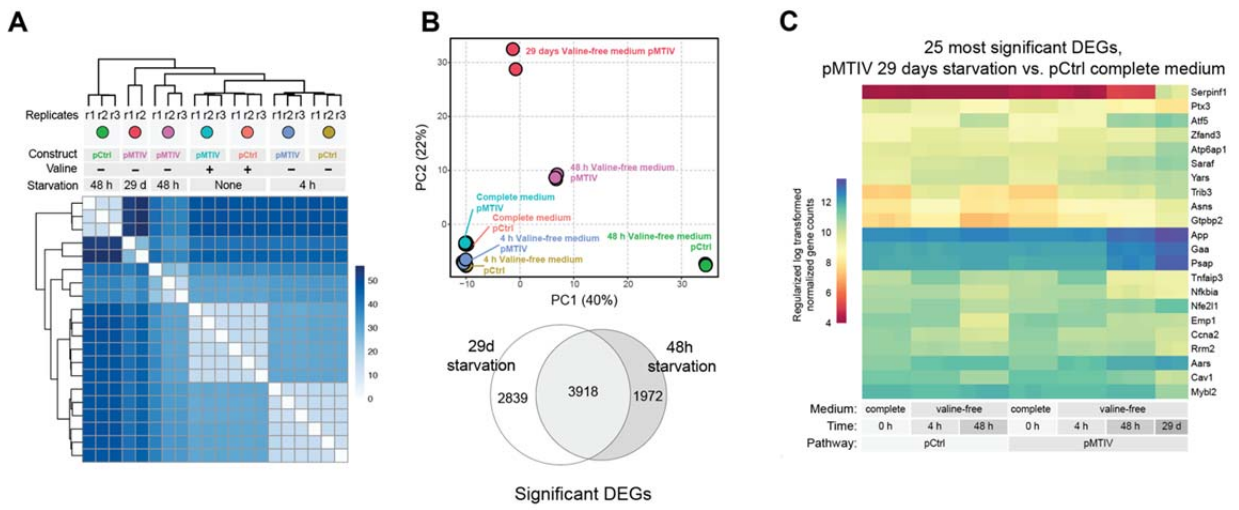

Figure 3 – figure supplement 5. Transcriptomic analysis of long-term (29 days) pMTIV pathway effect in conditioned valine-free F-12K medium.

(A) Regularized log transformed transcriptomic signatures of cells harboring the pMTIV or pCtrl constructs grown on complete F-12K medium or starved of valine for 4h, 48h, or 29d (5 passages). **(B)** A PCA plot of starved pMTIV and pCtrl cells, and Euler diagram of the overlap between DEGs from 29d of starvation and 48h starvation compared to pCtrl cells grown on complete F-12K medium. **(C)** A heatmap of the 25 most significant differently expressed genes between pMTIV cells starved of valine for 29 days and pCtrl cells grown on complete F-12K medium.

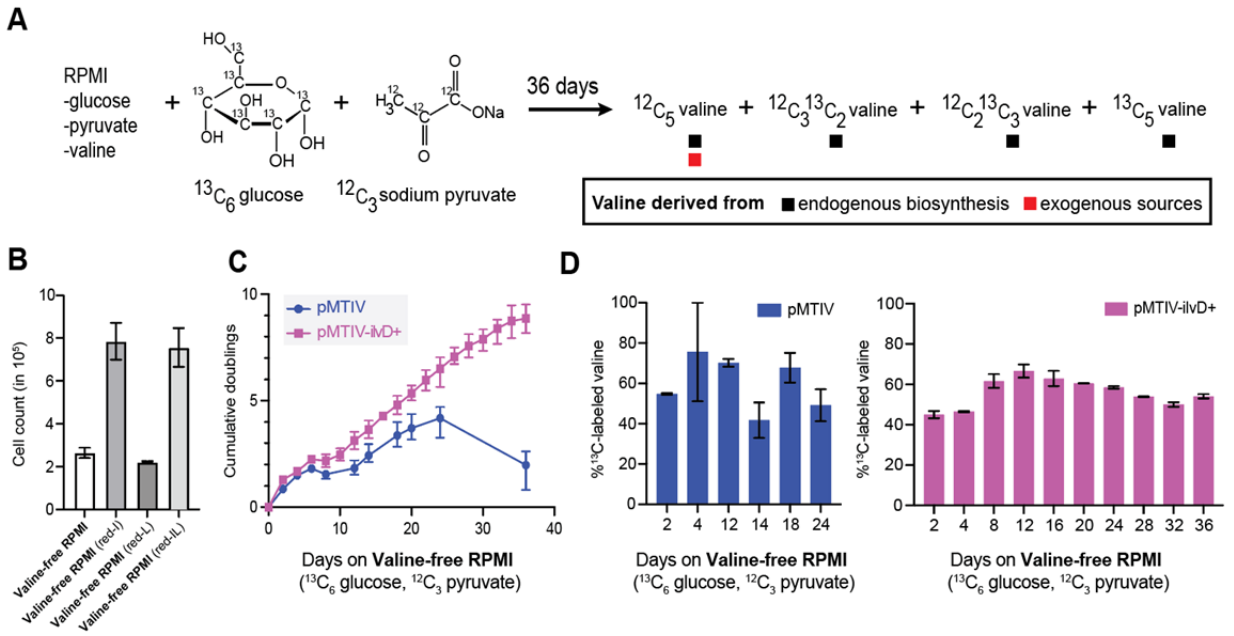

Figure 4 – figure supplement 1. Long-term culturing of cells in unconditioned isotopically heavy valine-free RPMI medium.

(A) Schematic outline of the ^{13}C-labeling strategy for detection of biosynthesized valine. Culturing regimen in isotopically heavy RPMI using $^{13}C_6$-glucose and $^{12}C_3$-sodium pyruvate should in principle result in the generation of $^{12}C_5$-valine (from 2 $^{12}C_3$ sodium pyruvate), $^{12}C_3{}^{13}C_2$ valine & $^{12}C_2{}^{13}C_3$ valine (from 1 $^{12}C_3$ and 1 $^{13}C_3$-sodium pyruvate), and $^{13}C_5$ (from 2 $^{13}C_3$-sodium pyruvate). **(B)** pMTIV cells cultured in valine-free RPMI (0.38 mM Ile, 0.38 mM Leu), reduced-isoleucine valine-free RPMI (0.06 mM Ile, 0.38 mM Leu), reduced-leucine valine-free RPMI (0.38 mM Ile, 0.2 mM Leu), and in reduced-isoleucine reduced-leucine valine-free RPMI (0.06 mM Ile, 0.2 mM Leu) **(Figure 4-figure supplement 1-source data 1)**. Triplicate values are plotted. **(C)** Population doubling level of pMTIV and pMTIV-ilvD+ cells cultured in isotopically heavy valine-free RPMI medium as described in (A). Triplicate values are plotted **(Figure 4-figure supplement 1-source data 1)**. **(D)** % of valine carrying at least one ^{13}C in pMTIV and pMTIV-ilvD+ cells cultured on unconditioned, reduced-isoleucine, valine-free RPMI medium containing $^{13}C_6$-glucose and 2 mM ^{12}C-sodium pyruvate on plates coated with 0.1% gelatin. Duplicate values are plotted **(Figure 4-figure supplement 1-source data 1)**

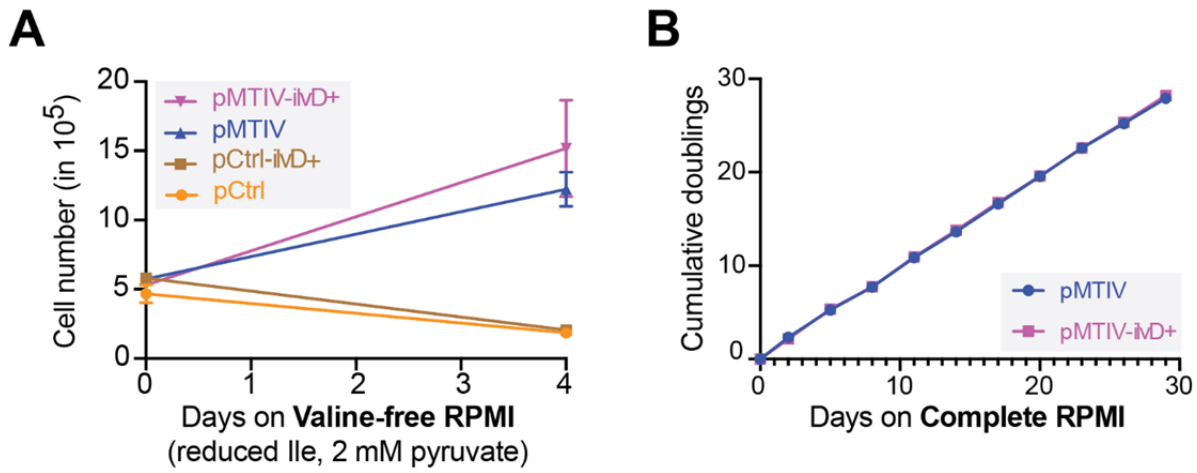

Figure 5 – figure supplement 1. Comparing growth of cell lines with elevated *ilvD* copy numbers to those without

(A) Comparison of growth in unconditioned reduced-isoleucine valine-free RPMI containing 2 mM sodium pyruvate **(Figure 5-figure supplement 1-source data 1)**. Triplicate values are plotted. **(B)** Comparison of pMTIV and pMTIV-ilvD+ long-term growth in reconstituted complete RPMI **(Figure 5-figure supplement 1-source data 1)**. Triplicate values are plotted.

SUPPLEMENTARY FILES

Supplementary file 1. Table of minimal prototrophic pathways set for AA prototrophy in mammalian cells.

Supplementary file 2. Protein sequences for each gene listed in Supplementary file 1.

Supplementary file 3. Codon-optimized nucleotide sequence for each gene listed in Supplementary file 1.

Supplementary file 4. Complete amino acid prototrophy pathway EC numbers.

SOURCE DATA FILES

Figure 1-figure supplement 1-source data 1. Raw cell count data for amino acid dropout curves.

Figure 1-figure supplement 2-source data 1. Raw and processed data for proline auxotrophy rescue by *proAB* construct.

Figure 2-source data 1. Raw cell count data for pMTIV valine-free and complete F-12K medium tests.

Figure 2-figure supplement 2-source data 1. Raw and annotated images of assembly junction PCR gel.

Figure 2-figure supplement 2-source data 2. Raw and annotated images of 2A Western blot.

Figure 2-figure supplement 3-source data 1. Raw and processed MS/MS data for dialyzed FBS amino acid measurements.

Figure 2-figure supplement 4B-source data 1. Raw PrestoBlue assay values for MTIV construct methionine, threonine and isoleucine dropout tests.

Figure 2-figure supplement 5-source data 1. Raw cell count data for pCtrl and pMTIV cells cultured in 50% conditioned valine-free F-12K medium.

Figure 2-figure supplement 6-source data 1. Raw cell count data for pIV valine-free and complete F-12K medium tests.

Figure 3-source data 1. Raw MS/MS data for ^{13}C valine labeling experiments.

Figure 3-figure supplement 1-source data 1. Further raw MS/MS data for ^{13}C valine labeling experiments.

Figure 4-source data 1. Control and ilvD qPCR data for pMTIV and pMTIV-ilvD+ cells, raw cell count data for pMTIV cultured in valine-free RPMI with different BCAA concentrations, and MS/MS data for long-term pMTIV and pMTIV-ilvD+ ^{13}C valine labeling experiments.

Figure 4-figure supplement 1-source data 1. Growth curve and MS/MS data for long-term pMTIV and pMTIV-ilvD+ ^{13}C valine labeling experiments.

Figure 5-source data 1. Raw and processed cell count data for pMTIV and pMTIV-ilvD+ cultured long-term in unconditioned valine-free RPMI medium.

Figure 5-figure supplement 1-source data 1. Raw cell count data for pCtrl, pMTIV, pCtrl-ilvD+ and pMTIV-ilvD+ cultured in valine-free and complete RPMI medium.